

Fuzzy Dark Matter Less-complex Wormhole Structures in Extended Theories of Gravity

Z. Yousaf,^{1,*} Kazuharu Bamba,^{2,†} Bander Almutairi,^{3,‡} M. Z. Bhatti,^{1,§} and M. Rizwan,^{1,¶}

¹*Department of Mathematics, University of the Punjab, Quaid-i-Azam Campus, Lahore-54590, Pakistan.*

²*Faculty of Symbiotic Systems Science, Fukushima University, Fukushima 960-1296, Japan.*

³*Department of Mathematics, College of Science, King Saud University, P.O. Box 2455 Riyadh 11451, Saudi Arabia.*

Fuzzy dark matter wormhole solutions coupled with anisotropic matter distribution are explored in 4D Einstein-Gauss-Bonnet and $f(R)$ gravity, where R is the Ricci scalar. We derive the shape function for fuzzy wormholes and explore their possible stability. We study the embedding diagrams of the active gravitational mass associated with fuzzy dark matter wormholes by taking a certain shape function. Aiming to highlight the role of Einstein-Gauss-Bonnet and $f(R)$ gravity in the modeling of less complex fuzzy wormhole structures, we evaluate the complexity factor, the conservation equation, and null energy conditions. Our study reinforces more importance of uniformly distributed pressure effects throughout the less complex region than to the emergence of energy density homogeneity in the stability of fuzzy wormholes. It is shown that the active gravitational mass of the fuzzy wormhole structures varies inversely with the radial distance thereby suggesting the breaching of energy conditions at some arena of Einasto index. Furthermore, it is revealed that stable fuzzy dark matter wormhole structures exist in nature in the surroundings of cold dark matter halos and galactic bulges. The important physics understood from our analysis is that in both four-dimensional Einstein-Gauss-Bonnet and $f(R)$ gravity, feasible geometries of fuzzy dark matter wormholes exist naturally in the environments of different galactic haloes.

I. INTRODUCTION

There are very unique solutions to Einstein's field equations that illustrate the relationship between two extremely remote regions or parallel universes, among the many solutions that the equations have to describe cosmological events. Originally dubbed as the Einstein-Rosen bridge [1], these structures were initially conceived to elucidate basic particles such as electrons through space-time tunnels interlaced with electric lines of force, or more specifically, to answer the particle issue in general relativity (GR). However, the main issue was that these geometric constructions were not stable. This indicates that the bridge cannot stay open for an object (not even a photon) to pass through it. Following that, Morris and Thorne's [2] provided the necessary prerequisites for creating a traversable wormhole (WH) space-time (Wheeler [3] originated the term "WH"). The concept of a WH is primarily topological and global in nature, locally, it is described as a 2D spatial surface on an achronal hyper-surface referred to as a "throat." The Schwarzschild metric, which is maximally extended, is the most commonly encountered form of a WH metric. The intriguing and thrilling idea of time travel at least theoretically has been made possible by these things in a relatively short amount of time.

In the domain of GR, it is widely acknowledged that the presence of exotic matter, which defies the null energy condition (NEC), is essential for the formation of stable traversable WHs. The logic of the implication of this condition comes from principles of topological censorship in the background of asymptotically flat regions, leading to the exploitation of constraints to some extent in the exploration of distant realms or alternate dimensions. It is well-known that a major challenge in the study of gravitational interactions exists in the construction of traversable WH geometries using relativistic/exotic matter that acts per the energy criteria. Thus highlighting the complex interaction between mathematical possibilities and feasible restrictions in the investigation of WHs. Various researchers have investigated and suggested extensions in the Einstein gravity models to avoid certain observational constraints of GR. An instance of this modification involves the consolidation of exotic matter as a scalar field which is thought to be non-minimally coupled in certain scalar-tensor theories of gravity. Furthermore, the gravitational amalgams in

* Email: zeeshan.math@pu.edu.pk

† Email: bamba@sss.fukushima-u.ac.jp

‡ Email: baalmutairi@ksu.edu.sa

§ Email: mzaeem.math@pu.edu.pk

¶ Email: mrizwan.math@gmail.com

the theories that embody extra curvatures put forward alternative routes to cope with these challenges. This distinctive environment of gravitational theories describes our search to refine our perception of gravity and its implications [2, 4–8].

An isotropic pressure distribution in stellar structures implies a disparity between radial and tangential pressures. Factors like the presence of multiple fluids, a solid core, phase transitions, rotation, magnetic fields, viscosity, or superfluidity can introduce anisotropies in pressure within the fluid. Anisotropic solutions offer a plausible description of astrophysical entities, reflecting our comprehensive understanding of these objects. Lemaître was the first to elucidate pressure anisotropy in a perfect fluid sphere, while Bower and Liang [9] highlighted the significance of locally anisotropic pressure equations (EOS) in relativistic contexts in 1974. In regions of extremely high density, such as $\rho > 10^{16} \text{kg}/\text{m}^3$, nuclear matter may exhibit anisotropic properties, as demonstrated in Ruderman’s seminal work [10]. Several scholarly articles delve into the development of anisotropic solutions, underscoring the ongoing exploration of this phenomenon in astrophysical research [11, 12]. Recently, In Ref. [13] Herrera explored self-gravitating compact anisotropic objects to analyze the notion of the vanishing complexity factor. In doing so, a general expression of the mass function was presented. By utilizing this mathematical approach, Herrera intended to describe the behavior of the locally anisotropic gravitational stellar objects and investigated the possible use of the vanishing complexity factor in this direction [14–18].

Extended gravitational theories have been put forward to elucidate certain observable occurrences that General Relativity (GR) struggles to account for. Examples of such phenomena include cosmic accelerated expansion, dark energy, dark matter, massive pulsars, and super-Chandrasekhar white dwarfs, among others. The gravity theories like Einstein-Gauss-Bonnet (EGB) gravity, $f(R)$ and $f(\mathcal{T})$, where R and \mathcal{T} represent the Ricci and torsion scalars, offer potential explanations for these phenomena (for more understanding, see Refs. [19–30]). The conventions that apply to matter generally do not hold in these situations. Instead, the geometry of the situation is taken into account, effectively replacing the need for exotic matter. The efficient field theories and the terms involving higher-order curvature is very important to accomplish this, which can be mathematically represented as extensions to the traditional Hilbert-Einstein Lagrangian. By taking this approach, the properties of WHs can be mimicked, providing a potential solution to the problem at hand [2, 4–8].

Black holes (BH) within $f(R)$ gravity models, exhibiting both constant and varying Ricci curvature, either in a vacuum or interacting with electrodynamics, have been documented in [31–42]. In the meanwhile, scalar fields are coupled as the matter content in $(3 + 1)$ and $(2 + 1)$ -dimensional $f(R)$ gravity scenarios in Refs. [43–45], with further analysis of the resulting BH solutions. For cosmological applications, this particular framework of $f(R)$ gravity coupled with non-minimally interacting scalar fields has already been investigated [46, 47].

The $f(R)$ theory led to the invention of WH solutions [48], in which the matter within the WH obeys the energy criteria and the violation of these conditions is due to the higher-order terms in $f(R)$ model of gravity. Bejarano *et al.* [49] studied thin-shell WHs with spherical symmetry in $(2 + 1)$ -dimensional $f(R)$ models of gravity, where the Ricci scalar is constant. In addition, Ref. [50] presents an analysis of the stability of thin-shell $(3 + 1)$ -dimensional WHs in $f(R)$ model of gravity including charge and constant curvature. In the realm of quadratic $f(R)$ model, Lorentzian spherically symmetric WHs with a constant scalar curvature have been discovered [50]. The Karmarkar condition has been utilized to examine WH geometries in various $f(R)$ models [51]. In Ref. [52], WHs having kinetic curvature scalar are examined. Moreover, WHs in the massive $f(R)$ model of gravity have been studied using several red-shift function behaviors in [53]. In the field of gravitational physics, researchers frequently employ the concept of anisotropic pressure as a fluid approximation when investigating self-gravitational fluid structures. Solving the gravitational equations related to non-static and static anisotropic spheres of fluid has been the subject of many studies. Many studies have been conducted on the hydrodynamical consequences of pressure showing local anisotropy and its applicability in the context of altered gravitational models. Anisotropies in fluids can result from a variety of things, including rotation, different kinds of phase transitions, magnetic fields, II-type superconductors, viscosity, solid cores, and P-type superfluids [11, 12, 54].

The study to explore WH geometries has been a central point in modified theoretical theories, like Einstein-Gauss-Bonnet (EGB) and Lovelock theories [55–57]. It is noteworthy that the EGB theory has been a source of research by many researchers to understand various hidden features of our enigmatic universe [58–61]. One may examine the effects of higher-dimensional curvature terms on spacetime structure by studying WHs in the EGB model. This theory was initially put forward by Lanczos and later independently redeveloped by David Lovelock. Extensively researched, the EGB gravity is a subject of significant study due to its derivation in String theory’s low-energy

domain, its stability when perturbed around flat space-time, and its capacity to generate nontrivial gravitational self-interactions without ghost-like instabilities [62–66]. It is established that $F(R, \mathcal{G})$ model of gravity suffer from ghost degrees of freedom, which can manifest at various levels within the theory, including as perturbative propagating modes when analyzing cosmological perturbations. A ghost-free $F(R, \mathcal{G})$ model of gravity was analyzed in Ref. [67].

The EGB theory exhibits topological properties in 4D due to the GB Lagrangian being a total derivative, thus not influencing gravitational dynamics. To have non-trivial gravitational effects within the EGB theory, a dimensionality of $D \geq 5$ is necessary. Glavan and Lin [68] recently resolved this limitation by adjusting the GB coupling constant α to $\alpha/(D-4)$, allowing for significant dynamics in four dimensions when approaching the limit $D \rightarrow 4$. To be specific, it is useful to consider it as the 4D EGB gravity [69–73], notable for its unique feature of circumventing the implications of Lovelock’s theorem and sidestepping Ostrogradsky instability. It is important to note upfront that Tomozawa explored dimensional regularization of this theory with comparable outcomes [65, 74, 75]. The 4D EGB theory gained significant interest following the work of Glavan and Lin [68] (and referenced in), where they introduced static spherically symmetric vacuum black holes with unique characteristics. These black holes exhibit intriguing features such as singularity-free behavior, repulsive gravitational force at short distances, and the singularity is not reached by falling particles.

To accurately depict real-world galactic systems, a model must comply with specific criteria for its descriptive capabilities, as per Einasto [76]. First, a descriptive function is selected, with the density profile being a sensible choice since the density profile is the source from which the gravitational potential, cumulative mass profile, and surface mass density are obtained. A physical model must meet various requirements, such as the density profile being non-negative, finite, and decreasing smoothly to approach zero at larger radii. Furthermore, the descriptive functions cannot have jump gaps (or discontinuities), and some moments of the mass function, such as those defining the system’s effective radius, total mass, and central gravitational potential, must be finite. Several valid descriptive-functions families, including the well-aligned Einasto density profile (EDP), were proposed by Einasto [76]. Einasto [77] used the EDP to model M31. Einasto [78] then applied the model to some surrounding galaxies, including M87, M32, the Sculptor dwarfs and Fornax, M31, and the Milky Way. These models were composed of several parts, each of which represented distinct physically homogeneous stellar populations with a unique parameter set \mathcal{P}_0, h and n named as central density, scale length, and Einasto index, respectively. The formulation of EDP can be utilized as a viable approach for constructing fuzzy dark matter WH solutions.

Herrera and collaborators explored the key results of gravitational collapse within the context of the Israel-Stewart formalism, focusing on the analysis of viscous dissipation involving bulk shear viscosity [79]. In the context of post-quasi static approximations, Herrera investigated solutions for the relativistic self-gravitating collapse in environments characterized by dissipative energy effects [80]. Odintsov and Oikonomou [81] investigated the fluid dynamics of rotating celestial bodies and established unique connections between inflationary attractors and the characteristics of compact stars to achieve stable configurations [82]. Nojiri *et al.* [59] introduced additional gravitational interaction terms to study the transmission of gravitational waves. They aimed to propose a framework where spherical relativistic entities could generate gravitational wave velocities equivalent to the speed of light in a vacuum environment. Building upon the context provided, our exploration delves into the potential application of fuzzy WHs in characterizing compact self-gravitating structures. Our focus centers on utilizing the Einasto-density profile (EDP) model to describe dark matter (DM) haloes, facilitating the development of a feasible interaction between WHs and DM haloes. Specifically, we introduce the Einasto-density profile as a foundational framework for our theoretical representation of the fuzzy WH phenomenon. This investigation aims to bridge the realms of theoretical physics and astrophysical observations, offering insights into the intriguing interplay between WHs and dark matter distributions within the cosmos [83].

Furthermore, Herrera *et al.* [84] determined that the system of equations that brings about the true scenario of disappearing spatial gradients of energy density is a collapsing source that collapses self-gravitating and has an anisotropic matter distribution. Additionally, the complexity factor of astrophysical configuration under modified gravity has been discussed by Yousaf and coworkers in various contexts [85]. The main goal of this research is to introduce a theoretical model of a time-independent, spherically-symmetric WH based on FDM using the extended theories of gravity. The article is organized as follows: Section II introduces the basic framework of field equations along with essential definitions. Section III explores violations of the NEC. Section IV offers a concise overview of the EDP. Section V delves into conservation equations. Section VI discusses the impact of active gravitational mass, while section VII addresses the complexity factor. The final section presents the conclusions and a summary of the

discussion.

II. BASIC FORMALISM FOR WORMHOLE MODELS IN EXTENDED GRAVITY

In this section, we provide the mathematical formalism to describe WH models in two well-known extended theories of gravity. First, we describe our theoretical modeling in the 4D EGB model of gravity and then we present the equations related to $f(R)$ gravity.

A. 4D EGB model of gravity

This section will provide a concise introduction to the 4D EGB model of gravity. The action for the EGB background is defined as [68]

$$I_G = \int \sqrt{-g} \left(\frac{\alpha}{D-4} \mathcal{L}_{GB} + L_m + R \right) d^D x,$$

where L_m denotes the Lagrangian for matter, the variable g signifies the determinant of $g_{\mu\nu}$, while α stands for the GB coupling coefficient. This paper will present the discussion related to the scenario where $\alpha \geq 0$. The Lagrangian term \mathcal{L}_{GB} is defined as

$$\mathcal{L}_{GB} = -4R^{\tau\eta}R_{\tau\eta} + R^2 + R^{\tau\eta\alpha\beta}R_{\tau\eta\alpha\beta}. \quad (1)$$

On applying the variational technique concerning $g_{\tau\eta}$ on the equation described above, the following equation of motion results

$$G_{\tau\eta} + \frac{\alpha}{D-4} \mathcal{S}_{\tau\eta} = \mathcal{K} T_{\tau\eta}, \quad (2)$$

where $T_{\tau\eta}$ is stress-energy momentum tensor and is defined as $T_{\tau\eta} = \frac{-1}{\sqrt{-g}} \frac{\delta(\sqrt{-g}L_m)}{\delta g^{\tau\eta}}$ and

$$G_{\tau\eta} = R_{\tau\eta} - \frac{1}{2} R g_{\tau\eta},$$

$$\mathcal{S}_{\tau\eta} = 4 \left(\frac{1}{2} R R_{\tau\eta} - R_{\tau\alpha} R_{\eta}^{\alpha} - R_{\tau\alpha\eta\beta} R^{\alpha\beta} - \frac{1}{2} R_{\tau\alpha\beta\gamma} R^{\alpha\beta\gamma}{}_{\eta} - \frac{1}{8} \mathcal{L}_{GB} g_{\tau\eta} \right).$$

In the context of four-dimensional space-time, the GB term is typically associated with the total derivative, leading to no discernible impact on the field equations. Yet, when adjusting the coupling constant to $\frac{\alpha}{D-4}$, the GB term remains non-zero for $D = 4$, allowing for further exploration of its contribution.

This article aims to investigate how anisotropic pressure influences the presence of fuzzy WH. The approach involves considering anisotropic matter distribution as a relativistic source, represented mathematically as follows

$$T_{\tau\eta} = (\rho + P_t) v_{\tau} v_{\eta} - P_t g_{\tau\eta} + \varrho \varkappa_{\tau} \varkappa_{\eta}, \quad (3)$$

where ρ stands for the fluid density, the variable $\varrho = P_r - P_t$, P_r and P_t are radial and tangential pressure components respectively. Additionally, the velocity-four vector v_{τ} and the radial unit-four vector \varkappa_{τ} adhere to the following conditions within the co-moving coordinate system: $v^{\tau} v_{\tau} = 1$ and $\varkappa^{\tau} \varkappa_{\tau} = -1$.

We now delve into the subject of fuzzy WHs with spherical symmetry. Our initial emphasis will be on examining the static spherically symmetric geometry [2]

$$ds^2 = g_{\tau\eta} dx^{\tau} dx^{\eta} = e^{2a(r)} dt^2 - \left(1 - \frac{b(r)}{r} \right)^{-1} dr^2 - r^2 d\Omega^2. \quad (4)$$

In the above expression $d\Omega^2 = d\theta^2 + \sin^2\theta d\phi^2$, the function $a(r)$ signifies a radial red-shift function, while $b(r)$ represents the shape function describing the geometry of the WH. In equation (3), the quantities v^{τ} and \varkappa^{τ} are

defined as $v^\tau = e^{-a(r)/2}\delta_0^\tau$ and $\varkappa^\tau = -\frac{1}{\sqrt{1-\frac{b(r)}{r}}}\delta_1^\tau$, respectively. To create stable surface structures resembling a WH's throat, it is essential to adjust the radial distance from a defined point r_0 to infinity. This modification is necessary to ensure the throat expands correctly, meeting the required flare-out conditions. Specifically, these conditions can be provided as $\frac{b(r) - rb'(r)}{b(r)^2} > 0$, with $b'(r_0) < 1$ and the prime symbol is denoting the derivative w.r.t. radial coordinate r . Within the EGB model framework, it is noteworthy that these limitations result in the creation of a WH associated with exotic matter, thereby breaching the NEC.

In the scenario where the $D \rightarrow 4$, the quantities associated with the matter, specifically denoted as ρ , P_r , and P_t , are explicitly represented as

$$\rho = \frac{1}{r^6}(\alpha b(r)(2rb'(r) - 3b(r)) + r^4 b'(r)), \quad (5)$$

$$P_r = \frac{1}{r^6} \left(\alpha b(r) (4r(r - b(r))a'(r) + b(r)) + 2r^4(r - b(r))a'(r) - b(r)r^3 \right), \quad (6)$$

$$P_t = \frac{1}{2r^6} (ra'(r)(12\alpha b(r) + r^3 - 8r\alpha)(b(r) - rb'(r)) + (r^3 - 2b(r)\alpha)(2r(r - b(r))a'(r) - rb'(r)) + 2r^2(r - b(r))(4b(r)\alpha + r^3)(a''(r) + a'(r)^2) - 4\alpha b(r)^2). \quad (7)$$

Equations (5)-(7) represent the field equations involving five unknown variables: ρ , P_r , P_t , $a(r)$, and $b(r)$. There exist numerous techniques available for solving such equations. Here, we outline the suggested approach to tackle these field equations.

B. Basic Formalism and Field Equations in $f(R)$ Gravity

A particular alternative form of Einstein's GR is the $f(R)$ model of gravity, where R denotes the Ricci-scalar. This altered model of gravity encompasses various gravitational theories, each distinguished by a distinct Ricci-scalar function. The most basic rendition of this function is when it mirrors the scalar itself, effectively reverting to GR. The inclusion of a customizable function within $f(R)$ gravity seeks to offer versatility in elucidating the universe's structural formation and tackling the issue of late-time cosmic acceleration. Buchdahl [86] first proposed this concept, using f as a placeholder for the arbitrary function, and Starobinsky [87] extensively studied cosmic inflation using this gravity theory. This paper examines the WH geometry in the $f(R)$ model, whose action is expressed as

$$I = \int \sqrt{-g} \left(\frac{f(R)}{\mathcal{K}^2} + L_m \right) d^4x,$$

with $\mathcal{K}^2 = 1$, the matter Lagrangian density is denoted as L_m , and g symbolizes the determinant of $g_{\xi\psi}$ (i.e., metric tensor). Through the variation of the action concerning $g_{\xi\psi}$ and utilizing the metric formalism, one can deduce the field equations governing $f(R)$ model as

$$(R_{\xi\psi} - \nabla_\xi \nabla_\psi + g_{\xi\psi} \square)F - \frac{1}{2}f g_{\xi\psi} = T_{\xi\psi}. \quad (8)$$

The function f 's derivative with respect to the R is represented as F . By contracting Eq. (2), we can derive a new expression as

$$3\square F + RF - 2f = T. \quad (9)$$

By considering the trace of the energy-momentum tensor as $T = g_{\xi\psi} T^{\xi\psi}$ and performing the necessary contractions and rearrangements, one can derive the field equations relative to $f(R)$ model as

$$G_{\xi\psi} = R_{\xi\psi} - \frac{1}{2}R g_{\xi\psi} = T_{\xi\psi}^{ef}. \quad (10)$$

The right-hand side of Eq. (10) corresponds to the stress-energy momentum tensor, $T_{\xi\psi}^{ef}$, which is obtained from the curvature stress-energy tensor, $T_{\xi\psi}^c = \frac{1}{F} \left(\nabla_{\xi} \nabla_{\psi} - \frac{1}{4} (RF + \square F + T) g_{\xi\psi} \right)$ and $\hat{T}_{\xi\psi}^{(m)} = \frac{T_{\xi\psi}^{(m)}}{F}$, the stress-energy momentum tensor for matter is provided as $T_{\xi\psi}^{(m)}$. The tensor, which serves to describe the matter content within a WH, can be expressed as an anisotropic matter's distribution given in Eq. (3). The focus is on the $f(R)$ gravity model in the metric formalism, with metric coefficients that are not dependent on time. We use Morris-Thorne spacetime to find exact solutions for traversable wormholes without violating energy and pressure conditions. We propose the power-law form of $f(R)$, where $f(R) = f_0 R^{1+\lambda}$, and λ is a real number. By setting λ to zero, GR can be recovered. The study of $f(R)$ theories of gravity was prompted by the necessity to characterize the post and pre-cosmic histories of our universe. The latest cosmic observational data on the acceleration-deceleration transition of the post-universe served as the primary impetus for investigating these theories. This stipulation placed limitations on $f(R)$ models, enabling feasible options for $f(R)$ models. Such theoretical frameworks evade the Ostrogradski instability and do not include involvement from invariants of curvature besides R [65, 75, 88–91]. In this context, the energy density of matter is symbolized by the variable ρ . Meanwhile, the pressures experienced in the transverse and radial directions are represented as P_2 and P_1 , respectively. With constant red-shift function, field equations associated with $f(R)$ model of gravity are provided as

$$\rho = \frac{1}{r^2} \left(F(r) b'(r) \right), \quad (11)$$

$$P_r = \frac{1}{2r^3} \left(F'(r) \left(r b'(r) - b(r) \right) r + 2F''(r) (b(r) - r) r^2 - 2b(r) F(r) \right), \quad (12)$$

$$P_t = \frac{1}{2r^3} \left(F(r) \left(b(r) - r b'(r) \right) + 2F'(r) r (b(r) - r) \right). \quad (13)$$

The interior of the celestial bodies of the cosmos, like galaxies and clusters of galaxies, undergo evolution within a dynamic medium, indicating a non-linear phase. To comprehend the formation of their structure, it is essential to study their linear, quasilinear, or nearly linear phases. Analyzing the non-linear gravitational interactions by using traditional mathematical approaches is often challenging. Researchers have employed different assumptions and numerical methods to address this complexity. In this context, we will focus on a specific category of the $f(R)$ model, firstly introduced by Starobinsky [87]

$$f(R) = R + \alpha R^2. \quad (14)$$

The model in the above expression contains a parameter, denoted as α , which can take on any real value. When this parameter is assigned a value of zero, the model corresponds to the dynamics of GR. To obtain the specific solutions for this model, we are required to solve field equations for this particular case and then simplify the results accordingly

$$\rho = \frac{1}{r^2} \left((2\alpha R + 1) b'(r) \right), \quad (15)$$

$$P_r = \frac{1}{r^3} \left(\alpha \left(r b'(r) - b(r) \right) r - b(r) (2\alpha R + 1) \right), \quad (16)$$

$$P_t = \frac{1}{2r^3} \left((2\alpha R + 1) \left(b(r) - r b'(r) \right) + 4\alpha (b(r) - r) \right). \quad (17)$$

III. WORMHOLE SOLUTION

It is widely acknowledged that energy conditions are violated in time-independent, spherically symmetric, four-dimensional space-time setups. This breaching of ECs is a significant occurrence within this particular space-time context. The flaring-out conditions dictate the presence of these violations. Additionally, in theories involving higher dimensions, it is conceivable that the regions around the throat of a WH are the only locations where EC violations can be avoided or satisfied. These conditions in extended gravity can be expressed as follows

$$T_{\xi\sigma} \kappa^{\xi} \kappa^{\sigma} \geq 0, \quad (18)$$

when κ denotes a null vector. The null energy condition (NEC) can be expressed for an anisotropic fluid as

$$\rho + P_r \geq 0 \text{ and } \rho + P_t \geq 0.$$

The equations (5)-(7) provide the following relationships for NEC as

$$\rho + P_r = \frac{1}{r^6} \left((2\alpha b(r) + r^3) \left(r (2ra'(r) + b'(r)) - b(r) (2ra'(r) + 1) \right) \right), \quad (19)$$

$$\begin{aligned} \rho + P_t = \frac{1}{2r^6} & (rb(r)(r^2(1 - 2(r^2 - 4\alpha)a''(r)) - ra'(r)(12\alpha + 12\alpha b'(r) + r^2) \\ & - 2(r^4 - 4\alpha r^2)a'(r)^2 + 6\alpha b'(r)) + r^3(r(2r^2a''(r) + b'(r)) + a'(r)(2r^2 - \\ & (r^2 - 8\alpha)b'(r)) + 2r^3a'(r)^2) - 4\alpha b(r)^2(2r^2a''(r) + 2r^2a'(r)^2 - 4ra'(r) + 3)). \end{aligned} \quad (20)$$

The aforementioned equations show that the flare-out condition causes the NEC to be violated when $a'(r) = 0$. Equation (19) transforms at the throat of the WH (where $r = r_0$) as

$$\rho(r_0) + P_r(r_0) = \frac{1}{r_0^6} \left((2\alpha b(r_0) + r_0^3) \left(r_0 (2r_0a'(r_0) + b'(r_0)) - b(r_0) (2r_0a'(r_0) + 1) \right) \right). \quad (21)$$

By making use of Eqs. (15)-(17), we get NEC expression in $f(R)$ gravity are as under

$$\rho + P_r|_{f(R)} = \frac{(rb'(r) - b(r))(\alpha r + 2\alpha R + 1)}{r^3}, \quad (22)$$

$$\rho + P_t|_{f(R)} = \frac{r((2\alpha R + 1)b'(r) - 4\alpha r) + b(r)(4\alpha r + 2\alpha R + 1)}{2r^3}, \quad (23)$$

where the notation " $|_{f(R)}$ " indicates that the quantity is calculated in $f(R)$ gravity. The given equations suggest that the flaring-out condition outcomes in the breach of NEC. Specifically, Eq. (22) transforms the WH throat, where the radius r equals the throat radius r_0

$$\rho(r_0) + P_r(r_0)|_{f(R)} = \frac{(r_0b'(r_0) - b(r_0))(\alpha r_0 + 2\alpha R + 1)}{r_0^3}. \quad (24)$$

IV. EDP MODEL

To enhance our understanding of the mysterious components present in the cosmos, such as DM haloes surrounding galaxy clusters, it is essential to explore their characteristics more profoundly. The studies involving cosmological simulations that analyze the development of structures through N-body techniques reveal that distinct density models with three specific parameters can effectively characterize different dark matter haloes or galaxy clusters [42, 83, 92, 93]. A model that is commonly used for DM haloes is the EDP model, a three-dimensional adaptation of the Sérsic model [93–95]. This model is utilized in analyzing the central regions of spiral galaxies and the brightness of ancient cosmic structures [96]. The EDP model, with its three parameters, provides a more accurate representation of DM haloes compared to some special forms of the halo model, which is characterized by only two parameters [97]. The EDP displays a power-law format with a logarithmic slope [98, 99] as

$$\wp(r) = \frac{d \ln(\rho)}{d \ln(r)}(r) \propto r^{\frac{1}{n}}, \quad (25)$$

here n is known as the Einasto index and this parameter helps in defining some particular form of the EDP model. One can obtain a general density profile through the integration of this parameter [95] as

$$\ln \left(\frac{\rho(r)}{\rho_m} \right) = -c_n \left(\left(\frac{r}{r_m} \right)^{\frac{1}{n}} - 1 \right). \quad (26)$$

In this context, the symbol r_m represents the radius of the sphere containing half of the total mass, while c_n is a parameter that influences r_m , with $\rho_m = \rho_m(r)$ and $\rho_0 = \rho_m e^{c_n}$. The value of c_n is a fixed numerical value that ensures ρ_m accurately describes the radius enclosing half of the mass. It is essential to note that multiple parameterizations of the EDP exist, each introducing distinct sets of independent parameters. Within the domain of DM-haloes, a commonly adopted representation follows a specific structure as

$$\ln \left(\frac{\rho(r)}{\rho_{-2}} \right) = -2n \left(\left(\frac{r}{r_{-2}} \right)^{\frac{1}{n}} - 1 \right). \quad (27)$$

Here r_{-2} and ρ_{-2} represent the radius and density, respectively, while the density function $\rho(r)$ is directly proportional to r^{-2} . One can write

$$\rho(r) = \rho_0 e^{[-(\frac{r}{h})^{\frac{1}{n}}]}, \quad (28)$$

while the scale length h is specified as

$$h = \frac{r_m}{c_n^n} = \frac{r_{-2}}{(2n)^n}, \quad (29)$$

and the central density is provided as

$$\rho_0 = \rho_m e^{c_n} = \rho_{-2} e^{2n}. \quad (30)$$

The descriptive components of the model need to satisfy particular standards such as mass profile, gravitational potential, and surface mass density to faithfully depict actual galactic formations [76]. The choice of these descriptive functions forms the basis for accurately representing any galactic structure model. Since the density profile plays a vital role in each of these functions, it emerges as the most advantageous option in this context. For any value of r , the function $\rho(r)$ must remain finite and positive. It should exhibit a slow decrease, getting closer to zero as r moves farther and closer to infinity. The density functions ought to link with a system that exhibits finite multi-pole expansion, total mass, and effective radius. Smooth transitions should be displayed by these descriptive functions; jump discontinuities and other abrupt or sudden shifts should be avoided. Any model aiming to faithfully depict real-world galactic structure must fulfill these criteria. In the following, we shall calculate the value of the shape function that led to the form of the equations of state parameters in the subsequent theories.

A. Calculations of shape function and EOS in 4D EGB Gravity

The traversable WH are believed to breach the NEC due to their exotic matter content. A sustainable WH may be formed through a gradual collapse process. Another feasible approach is to assess the stability of a traversable WH with a sizable throat. The determination of $b(r)$ in 4D EGB gravity involves the analysis of Eqs. (5) and (28), leading to the derivation of the differential equation (DE) in a specific format as

$$\frac{\alpha b(r) (2rb'(r) - 3b(r))}{r^6} + \frac{b'(r)}{r^2} = \rho_0 e^{-(\frac{r}{h})^{1/n}}. \quad (31)$$

The function $b(r)$ can be derived by solving the provided DE as

$$b(r) = \pm \frac{r \sqrt{\frac{r^4}{2\alpha} + 2\alpha cr + 2h^3 n \rho_0 r}}{\sqrt{2\alpha}} - \frac{r^3}{2\alpha'}, \quad (32)$$

where the integration constant (c) in the above equation can be found by using $b(r_0) = r_0$ as under

$$c = \frac{\alpha + h^3 n \rho_0 r_0 \Gamma \left(3n, \left(\frac{r_0}{h} \right)^{1/n} \right) + r_0^2}{\alpha r_0}. \quad (33)$$

Thus $b(r)$ in 4D EGB gravity takes the form

$$b(r) = \frac{\pm \sqrt{\alpha} r \sqrt{r \left(\frac{r^3}{\alpha} + \frac{4\alpha}{r_0} + 4h^3 n \rho_0 \left(\Gamma \left(3n, \left(\frac{r_0}{h} \right)^{1/n} \right) - \Gamma \left(3n, \left(\frac{r}{h} \right)^{1/n} \right) \right) + 4r_0} - r^3}}{2\alpha}. \quad (34)$$

In this equation, there are two shape functions associated with the sign of (\pm) . We have verified the condition of asymptotic flatness for both shape functions, and the shape function with positive sign meets the required criteria, i.e., $\frac{b(r)}{r} \rightarrow 0$ as $r \rightarrow \infty$. The dynamics of the shape function are illustrated in Figs. 9 and 10 in Appendix B. In Fig. 9 (mentioned in Appendix B), the left graph demonstrates that at $r_0 = 0.5$, $b(0.5) = 0.5$. The right graph in Fig. 9 in Appendix B confirms the satisfaction of flaring-out conditions. Furthermore, Fig. 10 shows asymptotic flatness in the left graph. The right graph in Fig. 10 in Appendix B reveals the location of the WH throat at $r_0 = 0.5$, where the curve $b(r) - r$ intersects the radial axis.

To gain insight into the behavior of the GB parameter α , we have illustrated the characteristics of WH conditions using contour plots as depicted in Fig. 11 (mentioned in Appendix B). The analysis of Fig. 11 in Appendix B reveals that as α rises, the behavior of $b(r)$ intensifies in the vicinity of the WH throat. This suggests a clear correlation between α and the shape function near the WH throat. Furthermore, the right plot of Fig. 11 in Appendix B demonstrates that as α increases, the derivative of $b(r)$ is less than 1. For the previously derived shape function, the WH metric can be expressed as

$$ds^2 = dt^2 - \left(\frac{2\alpha - \beta_1 + r^2}{2\alpha} \right)^{-1} dr^2 - r^2 (d\theta^2 + \sin^2 \theta d\phi^2). \quad (35)$$

When we consider $a'(r) = 0$, the resulting values of P_r and P_t in 4D EGB gravity will become

$$P_r = \frac{r^3 + \frac{\alpha^2}{r_0} + \alpha r_0 - \beta_1 r + \alpha h^3 n \rho_0 \left(\Gamma \left(3n, \left(\frac{r_0}{h} \right)^{1/n} \right) - \Gamma \left(3n, \left(\frac{r}{h} \right)^{1/n} \right) \right)}{\alpha r^3}, \quad (36)$$

$$P_t = \frac{1}{2\alpha^3 \beta_1 r^3 r_0} ((2r^2 - 3\beta_1)(\alpha^2 + \alpha \rho_0 h^3 n (-r_0) (\Gamma \left(3n, \left(\frac{r}{h} \right)^{1/n} \right) - \Gamma \left(3n, \left(\frac{r_0}{h} \right)^{1/n} \right)) + 2r_0^2) + \alpha \rho_0 r_0 r^3 (\beta_1 - 2r^2) e^{(\frac{r}{h})^{1/n}} - r_0 r^3 (r^2 - \beta_1)), \quad (37)$$

where

$$\beta_1 = \sqrt{\alpha} \sqrt{r \left(\frac{r^3}{\alpha} + \frac{4\alpha}{r_0} + 4h^3 n \rho_0 \left(\Gamma \left(3n, \left(\frac{r_0}{h} \right)^{1/n} \right) - \Gamma \left(3n, \left(\frac{r}{h} \right)^{1/n} \right) \right) + 4r_0}. \quad (38)$$

The equations of state (EOS) for the tangential and radial directions are given by the following expressions

$$\mathcal{W}_r = \frac{P_1}{\rho}, \quad \mathcal{W}_t = \frac{P_2}{\rho}. \quad (39)$$

These equations represent the relationships between pressure, density, and the respective directions in the system and have the following mathematical representation in 4D EGB gravity as

$$\mathcal{W}_r = \frac{e^{(\frac{r}{h})^{1/n}} \left(r^3 + \frac{\alpha^2}{r_0} + \alpha r_0 - \beta_1 r + \alpha h^3 n \rho_0 \left(\Gamma \left(3n, \left(\frac{r_0}{h} \right)^{1/n} \right) - \Gamma \left(3n, \left(\frac{r}{h} \right)^{1/n} \right) \right) \right)}{\alpha \rho_0 r^3}, \quad (40)$$

$$\mathcal{W}_t = \frac{e^{(\frac{r}{h})^{1/n}}}{2\rho_0 \alpha^3 \beta_1 r^3 r_0} ((2r^2 - 3\beta_1)(\alpha^2 + \alpha \rho_0 h^3 n (-r_0) (\Gamma \left(3n, \left(\frac{r}{h} \right)^{1/n} \right) - \Gamma \left(3n, \left(\frac{r_0}{h} \right)^{1/n} \right)) + 2r_0^2) + \alpha \rho_0 r_0 r^3 (\beta_1 - 2r^2) e^{(\frac{r}{h})^{1/n}} - r_0 r^3 (r^2 - \beta_1))$$

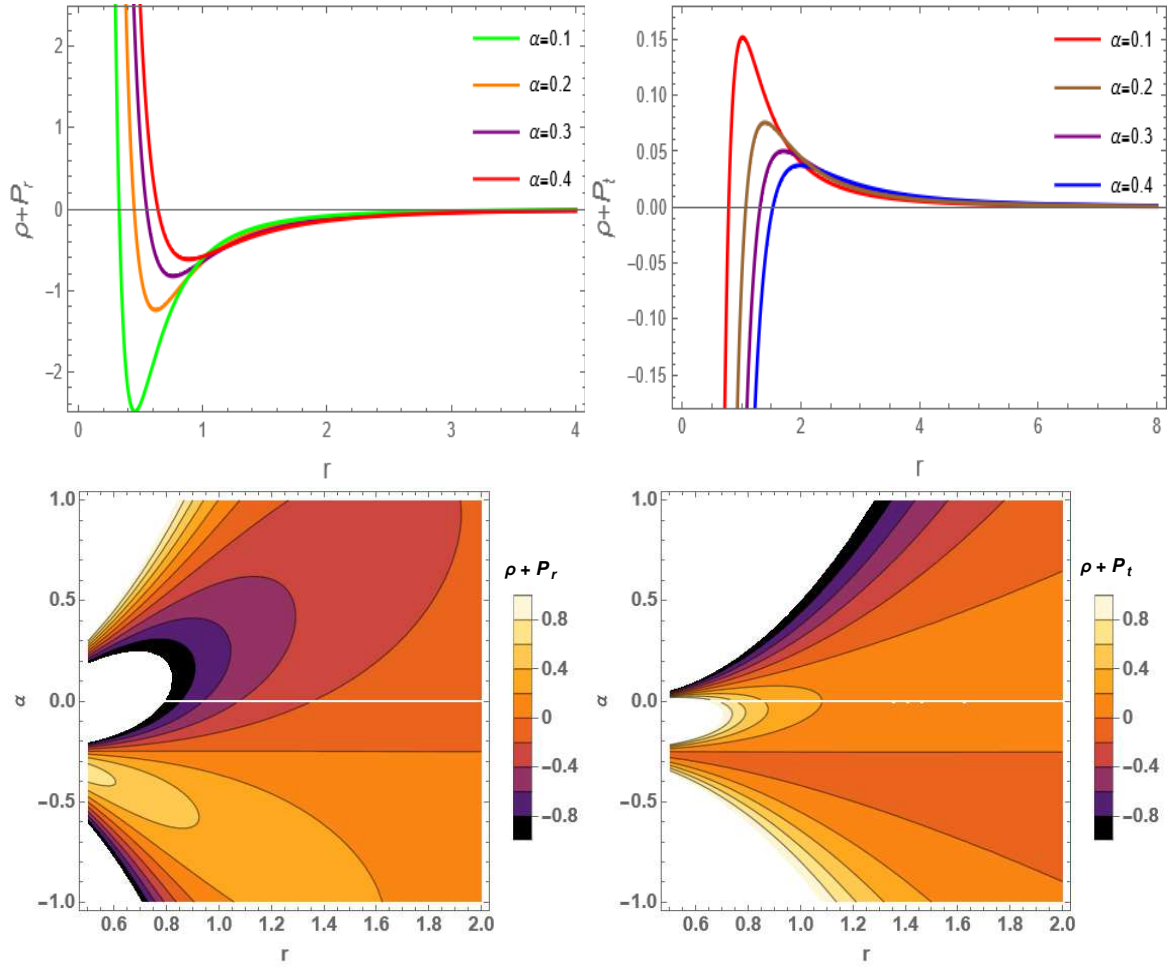


FIG. 1: The dynamics of $\rho + P_r$ and $\rho + P_t$ versus radial axis r corresponding to various α in 4D EGB theory.

$$- \Gamma \left(3n, \left(\frac{r_0}{h} \right)^{1/n} \right) + 2r_0^2) + \alpha \rho_0 r_0 r^3 (\beta_1 - 2r^2) e^{(\frac{r}{h})^{1/n}} - r_0 r^3 (r^2 - \beta_1)), \quad (41)$$

Figure 12 in Appendix B displays the graphs of \mathcal{W}_r and \mathcal{W}_t with respect to radial coordinate r . The behavior of \mathcal{W}_t is depicted on the left side of Fig. 12 in Appendix B. As \mathcal{W}_t approaches the WH-throat, it experiences a decrease, followed by an increase as it moves away from this location. The regions where the NEC conditions are satisfied, specifically when $\rho + P_r \geq 0$ and $\rho + P_t \geq 0$, have been identified and are visualized in Fig. 1.

B. Calculations of shape function and EOS in $f(R)$ Gravity

The calculation of $b(r)$ requires the examination of equations (15) and (23), which ultimately results in the development of a particular first-order differential equation in $f(R)$ gravity as

$$\frac{(2\alpha R + 1)b'(r)}{r^2} = e \left(-\left(\frac{r}{h} \right)^{\frac{1}{n}} \right) \mathcal{P}_0. \quad (42)$$

We consider the present values of the Ricci curvature scalar (i.e., $R = \tilde{R}$) and solve the above equation to find $b(r)$. The examination of constant curvature solutions within $f(R)$ model of gravity was carried out by Odintsov and his

associates and some researchers, as described in reference [100, 101]

$$b(r)|_{f(R)} = d - \frac{h^3 n \mathcal{P}_0 \Gamma \left(3n, \left(\frac{r}{h} \right)^{1/n} \right)}{2\alpha \tilde{R} + 1}. \quad (43)$$

The integration constant d , can be found by using the throat condition, i.e.,

$$b(r_0) = r_0,$$

which eventually yields in $f(R)$ gravity as

$$d = \frac{h^3 n \mathcal{P}_0 \Gamma \left(3n, \left(\frac{r_0}{h} \right)^{1/n} \right) + r_0 + 2\alpha r_0 \tilde{R}}{2\alpha \tilde{R} + 1}, \quad (44)$$

so the shape function will in $f(R)$ gravity become

$$b(r)|_{f(R)} = \frac{h^3 n \mathcal{P}_0 \left(\Gamma \left(3n, \left(\frac{r_0}{h} \right)^{1/n} \right) + \Gamma \left(3n, \left(\frac{r}{h} \right)^{1/n} \right) \right)}{2\alpha \tilde{R} + 1} + r_0. \quad (45)$$

How the shape function behaves within the background of $f(R)$ gravity is depicted in Figs. 13 and 14 in Appendix B. Figure 13 (mentioned in Appendix B) illustrates that $b(\frac{1}{2}) = \frac{1}{2}$, as shown in the left graph. The right graph in Fig. 13 confirms the substantiality of the well-known flaring-out limits. Moreover, Fig. 14 (right graph and is described in Appendix B) specifies the asymptotic flatness characteristics of the WH, while its left side graph points out that the locality of the WH throat is at $r_0 = \frac{1}{2}$, which is where the curve $b(r) - r$ intersects the radial axis. Moreover, Fig. 15 in Appendix B illustrates the variation of $b(r)$ within a particular range of Einasto index n near the WH throat within the background of $f(R)$ gravity. For the shape function derived above, metric will gain the following mathematical form

$$ds^2|_{f(R)} = dt^2 - \left(1 - \frac{1}{r(2\alpha \tilde{R} + 1)} \left(h^3 n \mathcal{P}_0 \Gamma \left(3n, \left(\frac{r_0}{h} \right)^{1/n} \right) + r_0 + 2\alpha r_0 \tilde{R} \right) \right)^{-1} dr^2 - r^2(d\theta^2 + \sin^2 \theta d\phi^2). \quad (46)$$

These equation of states of Eq. (39) provide the following relations in $f(R)$ gravity

$$\begin{aligned} \mathcal{W}_r|_{f(R)} &= \frac{-e^{(\frac{r}{h})^{1/n}} (\alpha r + 2\alpha \tilde{R} + 1)}{\mathcal{P}_0 r^3 (2\alpha \tilde{R} + 1)} \left(h^3 n \mathcal{P}_0 \left(\Gamma \left(3n, \left(\frac{r_0}{h} \right)^{1/n} \right) - \Gamma \left(3n, \left(\frac{r}{h} \right)^{1/n} \right) \right) + r_0 (2\alpha \tilde{R} + 1) \right) \\ &\quad + \frac{\alpha r}{\mathcal{P}_0 r^3 (2\alpha \tilde{R} + 1)}, \end{aligned} \quad (47)$$

$$\begin{aligned} \mathcal{W}_t|_{f(R)} &= -\frac{1}{2} - \frac{1}{2r^3 (2\alpha \tilde{R} + 1)} \left(h^3 n e^{(\frac{r}{h})^{1/n}} (4\alpha r + 2\alpha \tilde{R} + 1) \left(\Gamma \left(3n, \left(\frac{r}{h} \right)^{1/n} \right) - \Gamma \left(3n, \left(\frac{r_0}{h} \right)^{1/n} \right) \right) \right) \\ &\quad + \frac{e^{(\frac{r}{h})^{1/n}} \left(r_0 (4\alpha r + 2\alpha \tilde{R} + 1) - 4\alpha r^2 \right)}{2r^3 \mathcal{P}_0}. \end{aligned} \quad (48)$$

Figure 16 in Appendix B displays the graphs for \mathcal{W}_1 and \mathcal{W}_2 for a wide variety of galactic structures, including for cluster-sized haloes in the Millenium Run and the most massive haloes for the Millenium Simulation. As \mathcal{W}_1 approaches the WH-throat, it first rises and then decreases as it moves past this point. Figure 2 shows the regions where the NEC conditions, namely $\rho + P_1 \geq 0$ and $\rho + P_2 \geq 0$, are breached.

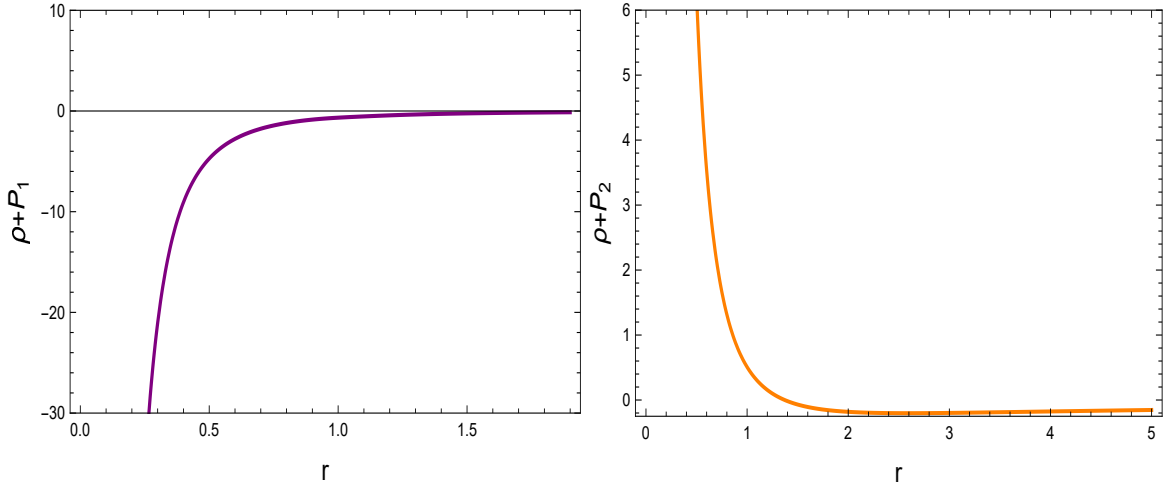


FIG. 2: NEC's behavior along radial coordinate r in $f(R)$ gravity.

V. EQUILIBRIUM SCENARIO AND ACTIVE GRAVITATIONAL MASS

In this section, we aim to determine the conservation equation for fuzzy WH solution through the application of a shape function derived from the EDP model. The equilibrium condition will be calculated using the generalized Tolman-Oppenheimer-Volkoff (TOV) equation provided as follow [102]

$$-\frac{dP_r}{dr} - \frac{a'(r)}{2}(\rho + P_r) - \frac{2}{r}(P_r - P_t) = 0. \quad (49)$$

This equation describes the equilibrium state achieved by WH configurations, taking into account forces that can be specified under

$$F_{gf} = -\frac{a'(r)}{2}(\rho + P_r), \quad (50)$$

$$F_{af} = -\frac{2}{r}(P_r - P_t), \quad (51)$$

$$F_{hf} = -\frac{dP_r}{dr}. \quad (52)$$

In this context, F_a , F_g , and F_h represent the anisotropic, gravitational, and hydrostatic forces, respectively. The state of equilibrium is achieved when the sum of these forces is zero, expressed as $F_{gf} + F_{af} + F_{hf} = 0$. Specifically, in our case, the gravitational forces are negligible, leading to a simplified equilibrium condition of $F_a + F_h = 0$. Through the application of $b(r)$, (i.e., shape function) resulting from the EDP model, the magnitude of the forces F_a and F_h have been calculated in EGB theory and are presented below

$$F_{af} = -\frac{(r^2 - \beta_2)^2}{\alpha r^5} + \frac{(\beta_2 - r^2)(r^2 - \beta_2)}{2\alpha r^5} + \frac{\beta_2 - r^2}{\alpha r^3} - \frac{(2r^2 - \beta_2) \left(\alpha^2 + r_0 \left(\alpha h^3 + \alpha h^3 n \rho_0 \Gamma \left(3n, \left(\frac{r_0}{h} \right)^{1/n} \right) + r^3 - r\beta_2 \right) + \alpha r_0^2 \right)}{\alpha^3 \beta_2 r^4 r_0}, \quad (53)$$

$$F_{hf} = \frac{1}{\alpha^3 \beta_2 r^4 r_0} (3\alpha^5 \beta_2 - 6\alpha^2 r^2 + r_0 (3\alpha^3 \beta_2 h^3 - 6\alpha h^3 r^2 + \alpha h^3 n \rho_0 (3\beta_2 - 6r^2) \Gamma(3n, (\frac{r_0}{h})^{1/n})) + r_0^2 (3\alpha^3 \beta_2 - 6\alpha r^2)), \quad (54)$$

where,

$$\beta_2 = \sqrt{\alpha} \sqrt{r \left(4h^3 n \rho_0 \Gamma \left(3n, \left(\frac{r_0}{h} \right)^{1/n} \right) + 4h^3 + \frac{r^3}{\alpha} + \frac{4\alpha}{r_0} + 4r_0 \right)}. \quad (55)$$

The analysis of the aforementioned forces has been conducted in EGB theory and illustrated in Fig. 3. The pa-

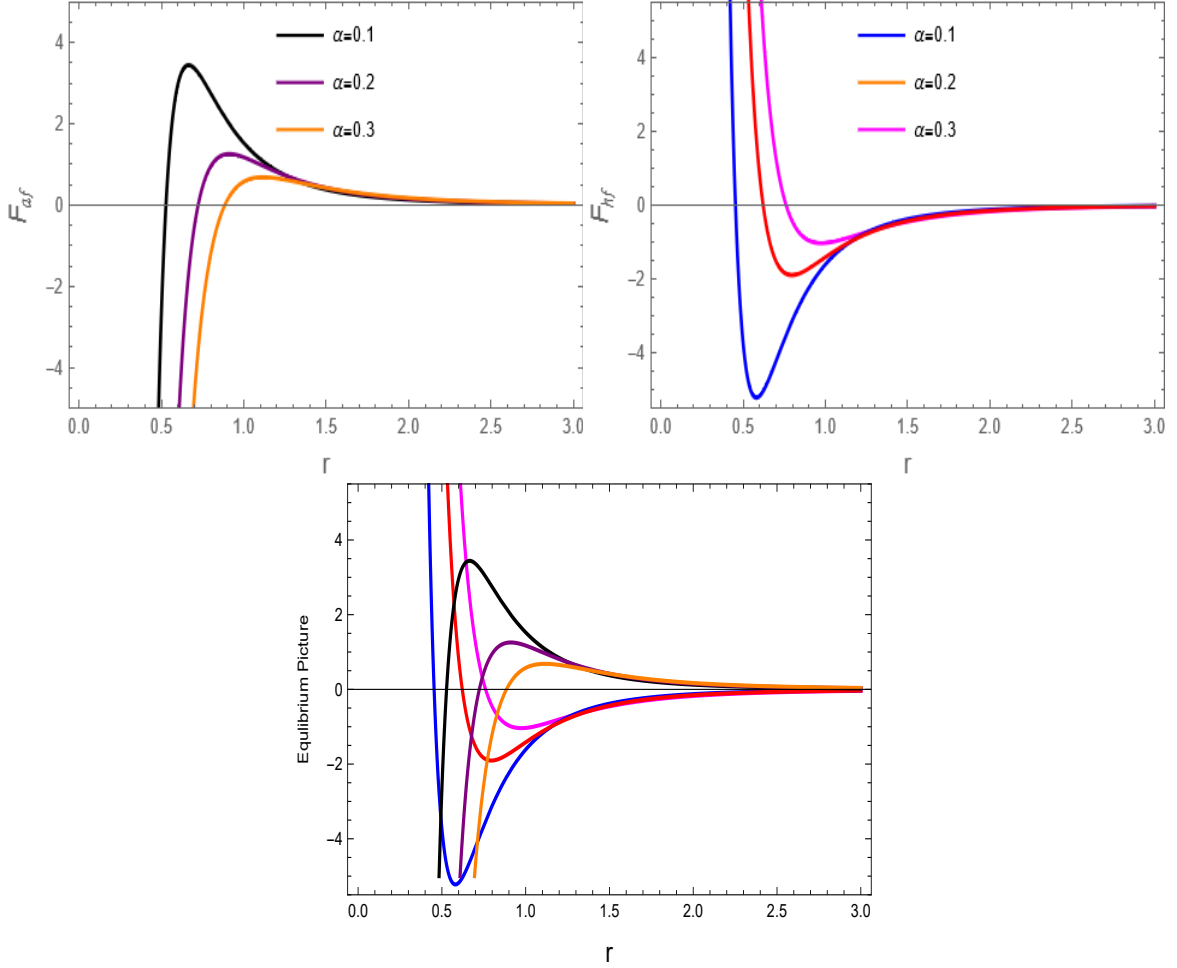


FIG. 3: The evaluation of equilibrium forces F_a and F_h versus r and equilibrium picture in 4D EGB theory.

rameters chosen for this study include $n = 0.5$, $r_0 = 0.5$, $h = 1$, and $\rho_0 = 0.01$. Upon examination of Fig. 3, it is noted that the forces F_a and F_h exhibit similar behaviors beyond $r = 2$ while acting in opposing directions. These forces appear to offset each other, indicating the potential existence of radially symmetric WH models that are not time-dependent. This inference was made based on graphs generated using specific parameter values that confirm previously discussed energy criteria in EGB theory.

The following expressions represent the magnitudes of the forces F_{af} and F_{hf} in $f(R)$ gravity as

$$F_{af}|_{f(R)} = \frac{\mathcal{P}_0 e^{-(\frac{r}{h})^{1/n}} (2\alpha(r + \tilde{R}) + 1)}{r^4 (2\alpha\tilde{R} + 1)} \left(-r^3 - 3h^3 n e^{(\frac{r}{h})^{1/n}} \left(\Gamma \left(3n, \left(\frac{r}{h} \right)^{1/n} \right) - \Gamma \left(3n, \left(\frac{r_0}{h} \right)^{1/n} \right) \right) \right) - \frac{1}{r^4} (4\alpha r^2 + r_0 (6\alpha(r + \tilde{R}) + 3)), \quad (56)$$

$$\begin{aligned}
F_{hf}|_{f(R)} = & \frac{\mathcal{P}_0 e^{-(\frac{r}{h})^{1/n}}}{r^4(n+2\alpha n\tilde{R})} \left(h^3 n^2 e^{(\frac{r}{h})^{1/n}} (2\alpha r + 6\alpha\tilde{R} + 3) \left(\Gamma\left(3n, \left(\frac{r}{h}\right)^{1/n}\right) - \Gamma\left(3n, \left(\frac{r_0}{h}\right)^{1/n}\right) \right) \right) \\
& + \frac{\mathcal{P}_0 e^{-(\frac{r}{h})^{1/n}}}{r^4(n+2\alpha n\tilde{R})} \left(\alpha r^4 \left(\left(\frac{r}{h}\right)^{1/n} - n \right) + n r^3 (\alpha r + 2\alpha\tilde{R} + 1) \right) - \frac{r_0}{r^4} (2\alpha r + 6\alpha\tilde{R} + 3). \quad (57)
\end{aligned}$$

It is worth mentioning that these equations describe the fundamental forces with the present Ricci scalar choices for the wide cluster ranges of dark matter halo objects with masses ranging from dwarfs to clusters. The forces

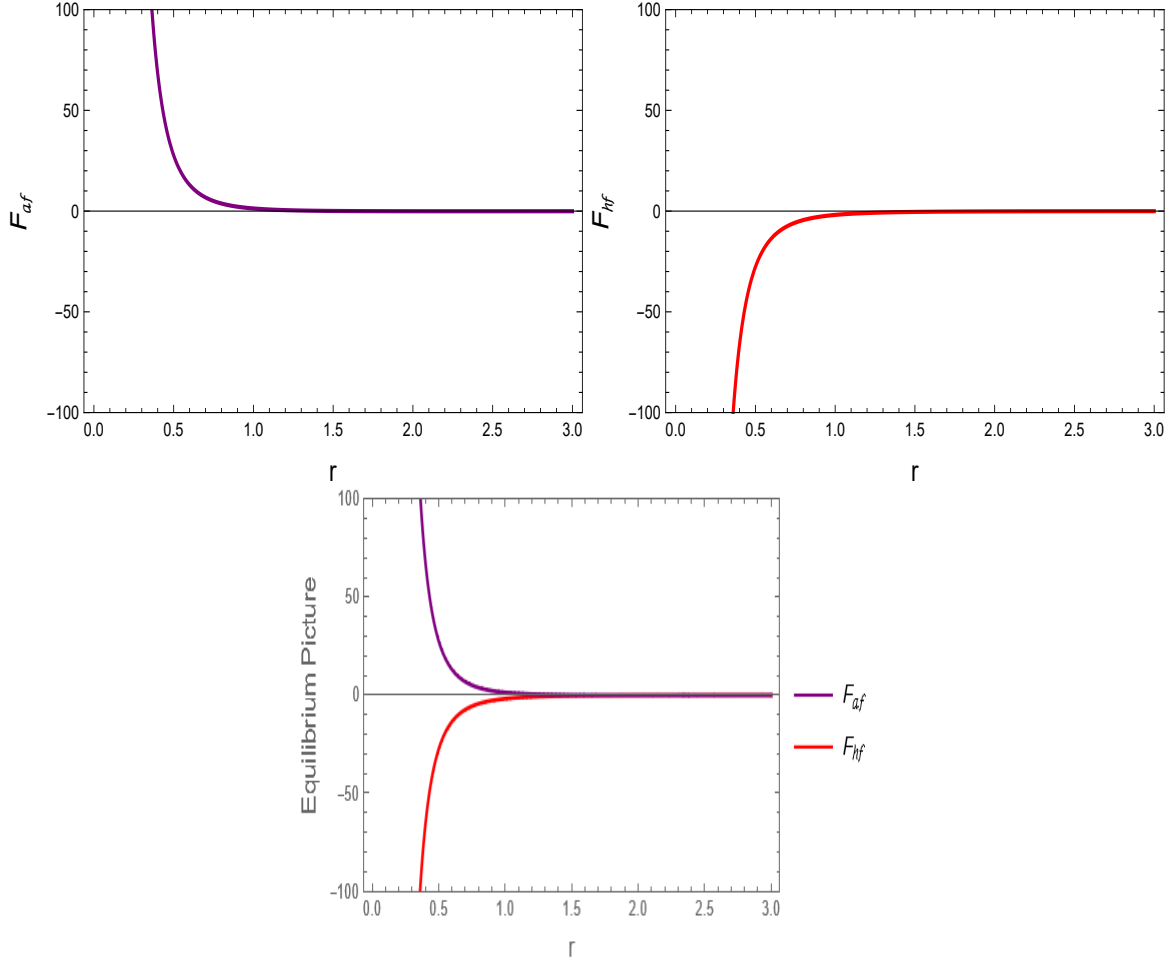


FIG. 4: The contribution of F_{af} and F_{ah} in the maintenance of equilibrium state of the fuzzy WH structure in $f(R)$ gravity.

discussed earlier have undergone analysis, and the outcomes are depicted in Fig. 4. The parameters considered in the study include $r_0 = 0.5$, $\alpha = 0.5$, $h = 1$, $\tilde{R} = 0.3$ and $\mathcal{P}_0 = 0.1$ in $f(R)$ gravity. The examination of Fig. 4 indicates that despite acting in opposing directions, forces F_{af} and F_{hf} exhibit similar behavior. These forces appear to counterbalance each other, hinting at the feasibility of time-independent radially symmetric WH models. By utilizing graphs generated with specific parameter values that satisfy the aforementioned energy criteria, this inference was drawn. This suggests that stable fuzzy dark matter WH structures exist in nature in the surroundings of cold dark matter DM halos and galactic bulges in $f(R)$ gravity.

We will discuss the active gravitational mass associated with fuzzy dark matter WHs. This mass is confined within the region of the WH from the initial throat radius r_0 to the boundary radius r . The active gravitational mass

(denoted by M_A) can be calculated using the following expression as

$$M_A = 4\pi \int_{r_0}^r \rho(r) r^2 dr. \quad (58)$$

For fuzzy anisotropic dark matter WHs, the gravitational mass expression is found in EGB theory as under

$$M_A = 4\pi h^3 n c_0 \left(\Gamma \left(3n, \left(\frac{r_0}{h} \right)^{1/n} \right) - \Gamma \left(3n, \left(\frac{r}{h} \right)^{1/n} \right) \right). \quad (59)$$

Figure 5 illustrates the behavior of M_A for fuzzy WH for a specific Einasto index $n = 0.5$ in EGB theory. The active gravitational mass M_A diminishes with increasing r due to the EDP in EGB theory. The existence of exotic matter is suggested when the active gravitational mass becomes negative in a particular spatial area, indicating a violation of energy conditions by this matter.

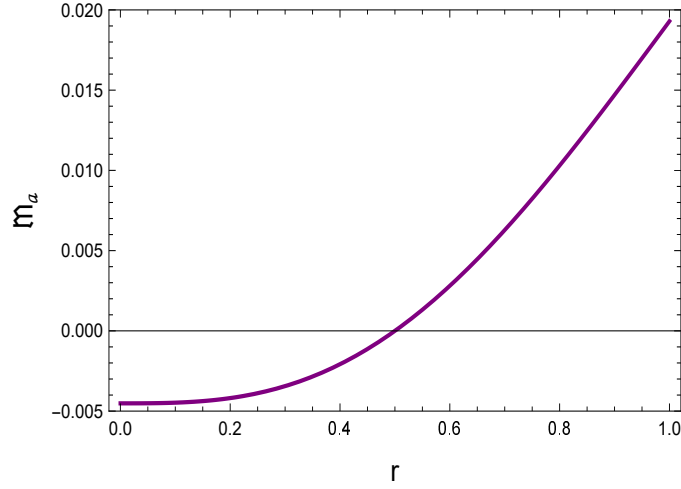


FIG. 5: The behavior of active gravitational mass of WH for $n = 0.5$, $h = 1$, $r_0 = 0.5$ and $\rho_0 = 0.01$ in 4D EGB theory.

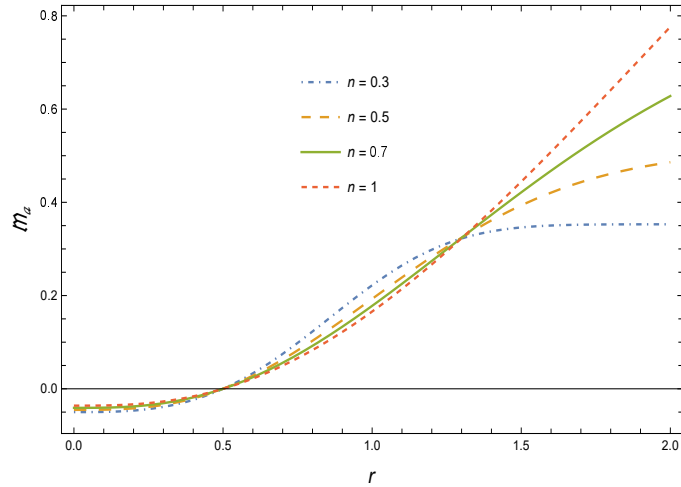


FIG. 6: The graphical analysis of active gravitational mass for various Einasto index n in $f(R)$ gravity.

For $f(R)$ gravity setup, the gravitational mass expression is found as under

$$\mathfrak{M}_a = 4\pi \mathcal{P}_0 \left(n r_0^3 E_{1-3n} \left(\left(\frac{r_0}{h} \right)^{1/n} \right) - n r^3 E_{1-3n} \left(\left(\frac{r}{h} \right)^{1/n} \right) \right), \quad (60)$$

where

$$E_{1-3n} \left(\left(\frac{r}{h} \right)^{1/n} \right), \quad (61)$$

is the exponent integral. Here, we denote the active gravitational mass in $f(R)$ with \mathfrak{M}_a . The behavior of \mathfrak{M}_a for fuzzy WH for different Einasto index n as shown in Fig. 6. Because of the EDP $f(R)$ gravity, the active gravitational mass \mathfrak{M}_a is negative near the wormhole throat. When the active gravitational mass in a given spatial region goes negative, it suggests the existence of exotic matter thereby implying that this stuff is violating NEC $f(R)$ gravity.

VI. COMPLEXITY FACTOR IN FUZZY WORMHOLE

Herrera proposed the concept of a complexity factor for time-independent, spherically symmetric compact objects in 2018 [13]. The notion of the complexity factor is predicated on systems that are simple or minimally complex and have uniform energy density and pressure that are isotropic. This sort of fluid distribution has a non-existent (or zero) complexity factor. The complexity factor for this kind of fluid distribution is used to study various cosmic stellar solutions including Bondi, axial metrics [14–18]. Furthermore, the complexity factor of systems comprising compact objects exhibiting anisotropic pressure and inhomogeneous energy density diminishes to zero as the individual impacts of these characteristics nullify each other [103–107]. The definition of the complexity factor is provided as follows [13]

$$\mathcal{Y}_{\mathcal{TF}} = (P_r - P_t) - \frac{1}{2r^3} \int_{r_0}^r r^3 \rho'(r) dr. \quad (62)$$

We have obtained a complexity factor of our system from the above formula in both EGB and $f(R)$ theories. After some manipulation, the final versions of the complexity factor are mentioned in Appendix A. The complexity trend of fuzzy dark matter WH along radial coordinate r for different values of GB parameter is depicted in Fig. 7 for EGB theory. In the background of $f(R)$ theory, the behavior is described in Fig. 8. It has been observed that as r moves towards infinity or away from the WH throat, $\mathcal{Y}_{\mathcal{TF}}$ tends towards zero. The lowest complexity factor signifies isotropic pressure and homogeneous energy density which justifies our results with [13]. Furthermore, non-uniform energy distribution and directional pressure can both be predicted by the zero complexity element until the opposing effects of these two elements achieve equilibrium in terms of complexity in EGB theory. Consequently, as one increases radial coordinates, $\mathcal{Y}_{\mathcal{TF}}$ drops towards zero, and the complexity element gradually grows towards the WH throat. In addition, the complexity dynamics place more importance on pressure uniformity than on energy density homogeneity.

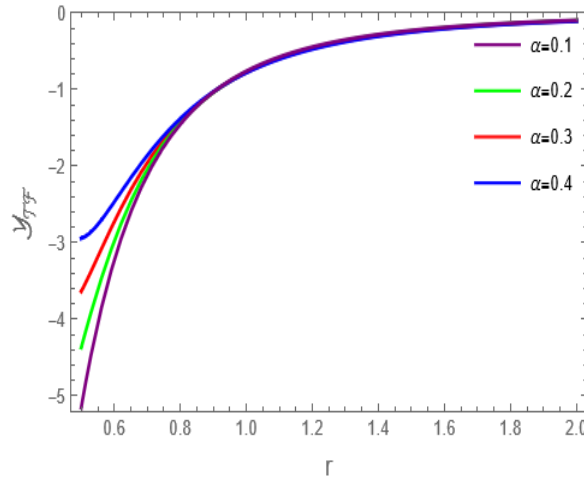


FIG. 7: The dynamics of complexity factor $\mathcal{Y}_{\mathcal{TF}}$ for different values of GB parameter α in 4D EGB theory.

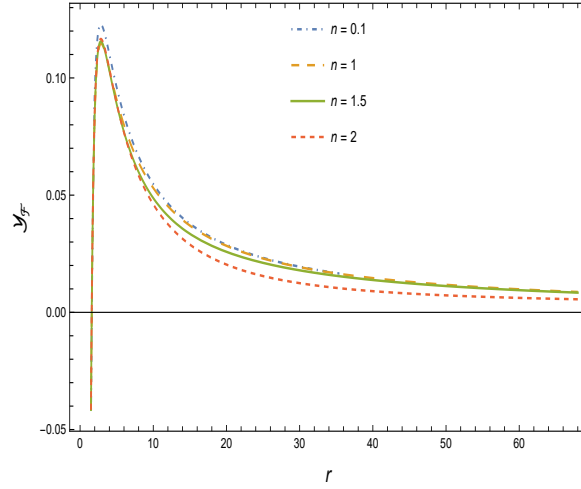


FIG. 8: The complexity factor's trajectory corresponds to different Einasto indices in $f(R)$ gravity.

VII. CONCLUSIONS

It is widely recognized that for a traditional WH model to be feasible, a crucial element must exist that violates the energy condition (EC) within the model's constraints. When examining modified gravitational models as a theoretical framework, the effective stress-energy tensor within WH passages adheres to ECs, potentially enabling the creation of distinct WH structures with additional curvature modifications. This research delves into the exploration of spherically symmetric fuzzy dark matter WH solutions linked to anisotropic matter distribution within the frameworks of 4D EGB and $f(R)$ models of gravity. Our involvement in EGB and $f(R)$ models stems from its significant coverage in the scientific literature concerning cosmic phenomena such as black holes, wormholes, and stellar formations. We have explored the potential for modeling central galactic structures using EGB and $f(R)$ models of gravity by proposing fuzzy WHs composed of DM. Our analysis has examined how the NEC impacts the distribution of matter content, particularly anisotropic fluids, to assess the influence of the EDP on the existence of WH models. In the existing literature, several established methods are available for analyzing WH models. One method involves hypothesizing the shape function for WH and studying ECs, while another method focuses on determining the shape function by assuming fluid components with strong coherence. By aligning the field equation with Einasto dark matter energy density and integrating the derived equation, the shape function is obtained. The evolution of the shape function is further examined and visually depicted through graphical representations (9, 10, 11, 13, 14 and 15, mentioned in Appendix B). Various plots have been created to highlight numerical outcomes related to the shape function, showcasing the adherence to throat and flare-out conditions, which are also visually illustrated. Through these figures, we conclude that the shape function derived from EDP could effectively define the geometry of the WH, as it satisfies the flare-out conditions, throat conditions, and flatness criteria in both EDP and $f(R)$ gravity.

The development of tangential and radial EOS has also been examined for the different choices of EGB. When an observer resides away from the WH throat, the value of \mathcal{W}_r decreases adversely, yet close to r_0 , we observe growing behavior. In contrast, a different pattern is observed with \mathcal{W}_t as described by Fig. 12 in Appendix B. The evolution of tangential and radial EOS has also been explored for a pattern of halo objects including cold dark matter halos, spiral galactic bulges, and cluster-sized haloes in the Millenium Run depending upon the choice of index n in $f(R)$ gravity. Away from the WH throat, the value of \mathcal{W}_1 decreases unfavorably, yet close to r_0 , an increasing pattern is observed. Conversely, a different pattern is observed with \mathcal{W}_2 as shown in Fig. 16 in Appendix B.

Numerous methods exist in the literature for studying WH configurations, including defining the shape function and analyzing the NEC. Our study focuses on NEC's behavior, revealing dissatisfaction at the WH throat ($r_0 = 0.5$) based on valid areas and NEC plots. An examination of the active gravitational mass indicates a negative value, implying the existence of exotic matter that contradicts ECs. Additionally, an analysis of the equilibrium forces for fuzzy WHs includes the computation of hydrostatic and anisotropic forces. The plots 1 and 2 demonstrate how they entirely cancel each other out. It is concluded that within a proper arena of parametric Einasto choices, the WEC

is dissatisfied thus indicating the occurrences of exotic matter for fuzzy dark matter WHs both in EGB and $f(R)$ gravity (indicated in Figs. 1 and 2).

We have performed an analysis of the equilibrium forces for fuzzy WHs by evaluating hydrostatic and anisotropic forces. The stable and well-sustained geometries of fuzzy dark matter WHs are available in nature under the effects of extra curvature $f(R)$ terms as described by Figs. 3 and 4. The contribution of active matter content quantity in producing gravitational interaction in EGB and $f(R)$ gravity keeps on increasing with the radial coordinate r in an atmosphere of a variety of astrophysical systems mediated by the Einasto index n . This can be well-justified from the Figs. 5 and 6.

We have taken into consideration the static irrotational spacetime metric of the WH and subsequently deduced the complexity factor, motivated by the work by Herrera [13]. The complexity factor of fuzzy dark matter WHs is calculated, displaying a consistent increase over time. On increasing the contribution of EGB theory controlled by α , the value of the complexity factor increases. Thus EGB theory is likely to host more complex systems. However, in the background of $f(R)$ theory indicates that the complexity takes on its role in the structure of WH and after attaining a specific radial coordinate value, (i.e., $r = 4.9$), the contribution of complexity reduces gradually. This clearly shows that less-complex WH geometric within the framework of specific halo objects exists, as an observer moves away from the central core of the spherical geometric objects in $f(R)$ gravity. The important physics understood from our analysis is that the realistic geometries of fuzzy dark matter WHs exist in nature in the surroundings of various galactic haloes in both EGB and $f(R)$ gravity. It would be worthwhile to analyze the complexity-free analysis for the diffused fuzzy black hole droplets by using our presented technique which could be our future work.

ACKNOWLEDGEMENT

The work of KB was partially supported by the JSPS KAKENHI Grant Number 21K03547 and 23KF0008. The work by BA was supported by Researchers Supporting Project number: RSPD2024R650, King Saud University, Riyadh, Saudi Arabia.

CONFLICT OF INTEREST

The authors declare no conflict of interest.

DATA AVAILABILITY STATEMENT

This manuscript has no associated data or the data will not be deposited. [Authors comment: This manuscript contains no associated data.]

APPENDIX A

The following complexity factor has been achieved by using the values of our under-considered system in Eq. (62). This is found for 4D EGB theory as

$$\mathcal{Y}_{TF} = -\frac{1}{2r^3} \left(-\frac{2 \left(r^3 + \frac{\alpha^2}{r_0} + \alpha r_0 - \beta_1 r + \alpha h^3 n \rho_0 \left(\Gamma \left(3n, \left(\frac{r_0}{h} \right)^{1/n} \right) - \Gamma \left(3n, \left(\frac{r}{h} \right)^{1/n} \right) \right) \right)}{\alpha} \right. \\ \left. + \frac{\left(2r^2 - 3\beta_1 \right) \left(\alpha^2 + \alpha \rho_0 h^3 n r_0 \left(\Gamma \left(3n, \left(\frac{r_0}{h} \right)^{1/n} \right) - \Gamma \left(3n, \left(\frac{r}{h} \right)^{1/n} \right) \right) + 2r_0^2 \right)}{\alpha^3 \beta_1 r_0} \right)$$

$$\begin{aligned}
& + \frac{\alpha \rho_0 r_0 r^3 \left(\beta_1 - 2r^2 \right) e^{-\left(\frac{r}{h}\right)^{1/n}} - r^3 r_0 \left(r^2 - \beta_1 \right)}{\alpha^3 \beta_1 r_0} \\
& + h^3 \rho_0 \left(\Gamma \left(3n + 1, \left(\frac{r}{h} \right)^{1/n} \right) - \Gamma \left(3n + 1, \left(\frac{r_0}{h} \right)^{1/n} \right) \right),
\end{aligned} \tag{63}$$

while for $f(R)$ gravity, it is found to be

$$\begin{aligned}
\mathcal{Y}_{\mathcal{F}|f(R)} &= \frac{1}{2r^3} \left(\mathcal{P}_0 r_0^3 \left(\frac{r_0}{h} \right)^{1/n} E_{-3n} \left(\left(\frac{r_0}{h} \right)^{1/n} \right) + \mathcal{P}_0 \left(-r^3 \right) \left(\frac{r}{h} \right)^{1/n} E_{-3n} \left(\left(\frac{r}{h} \right)^{1/n} \right) \right) \\
&+ \frac{\mathcal{P}_0 e^{-\left(\frac{r}{h}\right)^{1/n}} (2\alpha r + 2\alpha R + 1) \left(r^3 - 3h^3 n e^{\left(\frac{r}{h}\right)^{1/n}} \Gamma \left(3n, \left(\frac{r_0}{h} \right)^{1/n} \right) + 3h^3 n e^{\left(\frac{r}{h}\right)^{1/n}} \Gamma \left(3n, \left(\frac{r}{h} \right)^{1/n} \right) \right)}{2r^3 (2\alpha R + 1)} \\
&+ \frac{1}{2r^3} (4\alpha r^2 - 3r_0 (2\alpha r + 2\alpha R + 1)).
\end{aligned} \tag{64}$$

We evaluate a constraint for obtaining a less-complex WH structure by assigning a zero value to the above equation in our analysis.

APPENDIX B

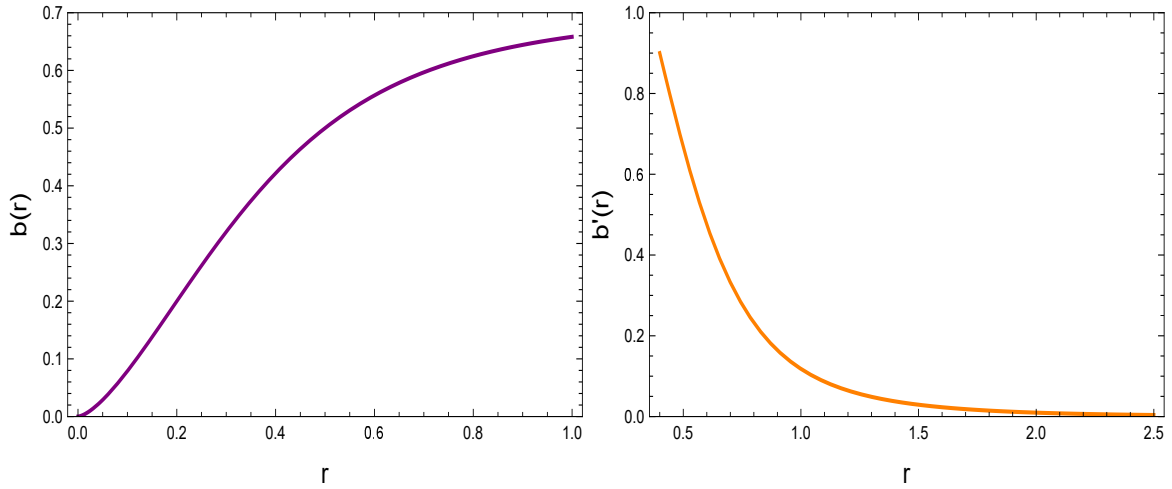


FIG. 9: The relation between $b(r)$ and r in 4D EGB theory is shown in the left figure. The picture on the right side displays the trajectory of $b'(r) < 1$. In this instance, $r_0 = 0.5$.

The left diagrams of Figs. 9, 13, 11 and 15 describe the diagrams of the shape function of the WH. One can notice elaborately the properties related to the structure of WH via these graphs. The location of the WH throat, where the radial coordinate achieves the least value, is shown by the graph's smallest value of $b(r)$. This also describes the transition of the WH from its neck to the surrounding space away from the throat (as r decreases or increases) in the subsequent theories. The minimum value of $b(r)$ in the same graph points to the throat size thereby providing more insights insight into the size and stability of the traversable WH epochs. The variations in the spherically symmetric WH radius (or its effective size) in both EGB and $f(R)$ theories versus if an observer moves along the radial direction can be visualized through the left graphs of Figs. 9, 13, 11 and 15. The rate of radial change in the shape function versus the radial coordinate is shown in the right diagrams of Figs. 9, 13, 11 and 15. No spikes and sudden variations in $b'(r)$ at certain values of r after including corrections from EGB and $f(R)$ theories are observed, thereby providing feasible and realistic WH features including throat's least radius or transitions in the geometry of WH. A smooth

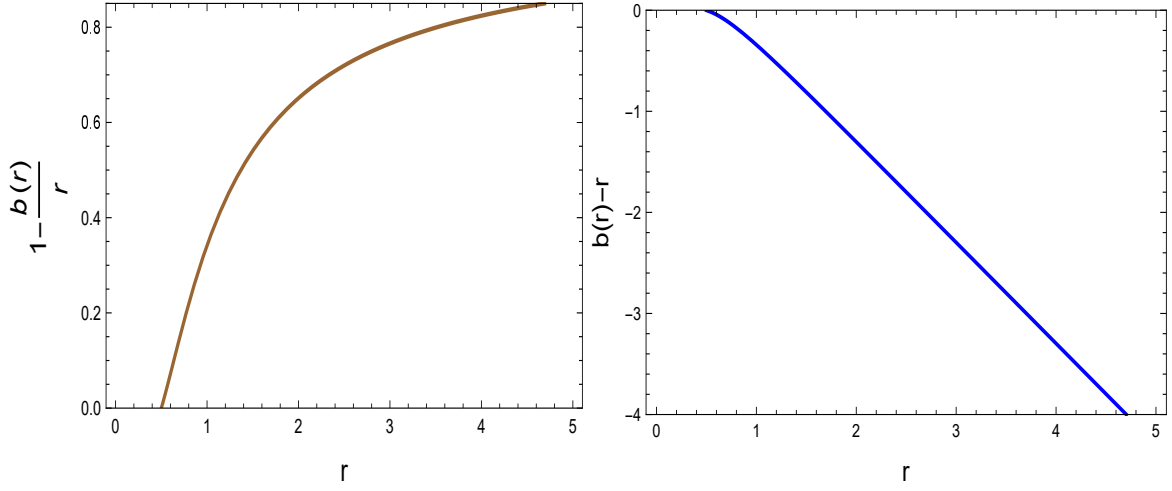


FIG. 10: The dynamics of $1 - \frac{b(r)}{r}$ and $b(r) - r$ versus r in 4D EGB theory.

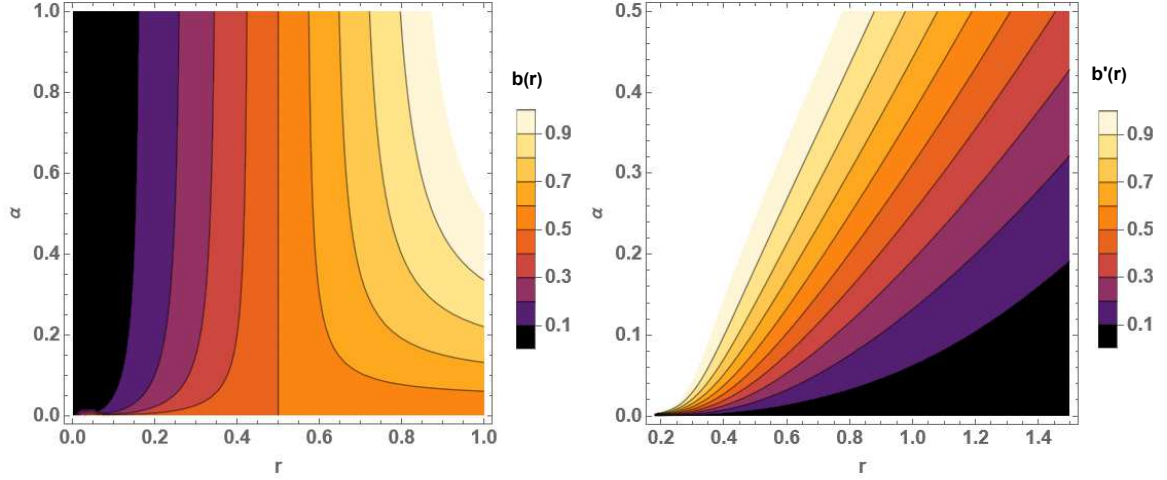


FIG. 11: The contour plots of $b(r)$ and $b'(r)$ corresponding to a particular α domain in 4D EGB theory.

and continuous trajectories of $b'(r)$ are noticed from the right diagrams of Figs. 9, 13, 11 and 15 thereby pointing out relatively stable WH with the potentially traversable geometry. The negative regions of $b(r) - r$ have been shown for certain radial coordinate values in Figs. 11 and 15. These graphs indicate that the observer observes a collapsing/pinching off of the spatial spherically symmetric dimensions when an observer moves away from WH throat, i.e., ($r > r_0$). This further leads to an understanding that our fuzzy dark matter WH is not traversable, thus reinforcing that some sort of exotic matter is required to stabilize WH geometry. This reveals the requirement of the exotic matter for its stability that would prevent our WH structure from collapsing. Figures 12 and 16 describe that \mathcal{W}_r and \mathcal{W}_t are within the feasible bounds. How the shape function behaves is depicted in Figs. 13 and 14. Figure 13 illustrates that $b(\frac{1}{2}) = \frac{1}{2}$, as shown in the left graph. The right graph in Fig. 13 confirms the substantiality of the well-known flaring-out limits. Moreover, Fig. 14 (right graph) specifies the asymptotic flatness characteristics of the WH, while its left side graph points out that the locality of the WH throat is at $r_0 = \frac{1}{2}$, which is where the curve $b(r) - r$ intersects the radial axis. Moreover, Fig. 15 illustrates the variation of $b(r)$ within a particular range of Einasto index n near the WH throat.

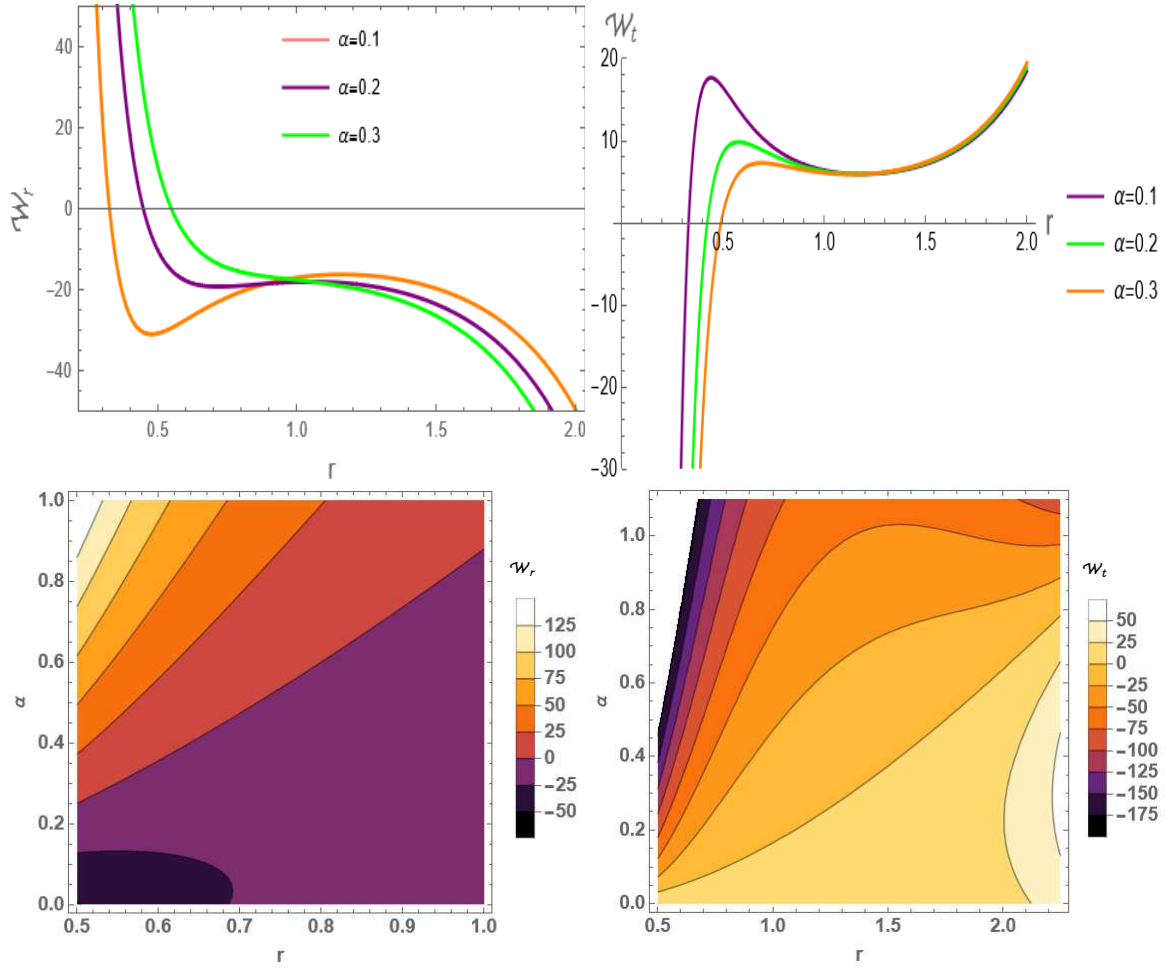


FIG. 12: The behavior of W_r and W_t along radial axis r for different choices of α in 4D EGB theory.

- [2] M. S. Morris and K. S. Thorne, Am. J. Phys. **56**, 395 (1988).
- [3] J. A. Wheeler, Phys. Rev. **97**, 511 (1955).
- [4] H. G. Ellis, J. Math. Phys. **14**, 104 (1973).
- [5] K. Bronnikov, Acta. Phys. Pol. p. B4 (1973).
- [6] G. Clement, Gen. Relativ. Gravit. **13**, 763 (1981).
- [7] M. Visser, *Lorentzian Wormholes. From Einstein to Hawking* (American Institute of Physics, 1996).
- [8] D. Hochberg and M. Visser, Phys. Rev. D. **58**, 044021 (1998).
- [9] R. L. Bowers and E. Liang, Astrophys. J. **188**, 657 (1974).
- [10] M. Ruderman, Annu. Rev. Astron. Astrophys. **10**, 427 (1972).
- [11] A. V. Astashenok, S. D. Odintsov, and V. K. Oikonomou, Symmetry **15**, 1141 (2023).
- [12] A. Malik, A. Qadeer, M. Ahmad, S. A. Mardan, and Z. Yousaf, Eur. Phys. J. Plus **139**, 101 (2024).
- [13] L. Herrera, Phys. Rev. D. **97**, 044010 (2018).
- [14] L. Herrera, A. Di Prisco, and J. Carot, Phys. Rev. D **99**, 124028 (2019).
- [15] L. Herrera, Phys. Rev. D **101**, 104024 (2020).
- [16] E. Contreras, E. Fuenmayor, and G. Abellán, Eur. Phys. J. C **82**, 187 (2022).
- [17] L. Herrera and A. Di Prisco, Phys. Rev. D **109**, 064071 (2024).
- [18] L. Herrera, A. Di Prisco, and J. Ospino, Phys. Rev. D **109**, 024005 (2024).
- [19] A. G. Riess, A. V. Filippenko, P. Challis, A. Clocchiatti, A. Diercks, P. M. Garnavich, R. L. Gilliland, C. J. Hogan, S. Jha, R. P. Kirshner, et al., Astron. J. **116**, 1009 (1998).
- [20] P. Ade, N. Aghanim, Z. Ahmed, R. Aikin, K. Alexander, M. Arnaud, et al., Phys. Rev. Lett. **114**, 101301 (2015).
- [21] D. J. Eisenstein et al., Astrophys. J. **633**, 560 (2005).
- [22] B. Jain and A. Taylor, Phys. Rev. Lett. **91**, 141302 (2003).

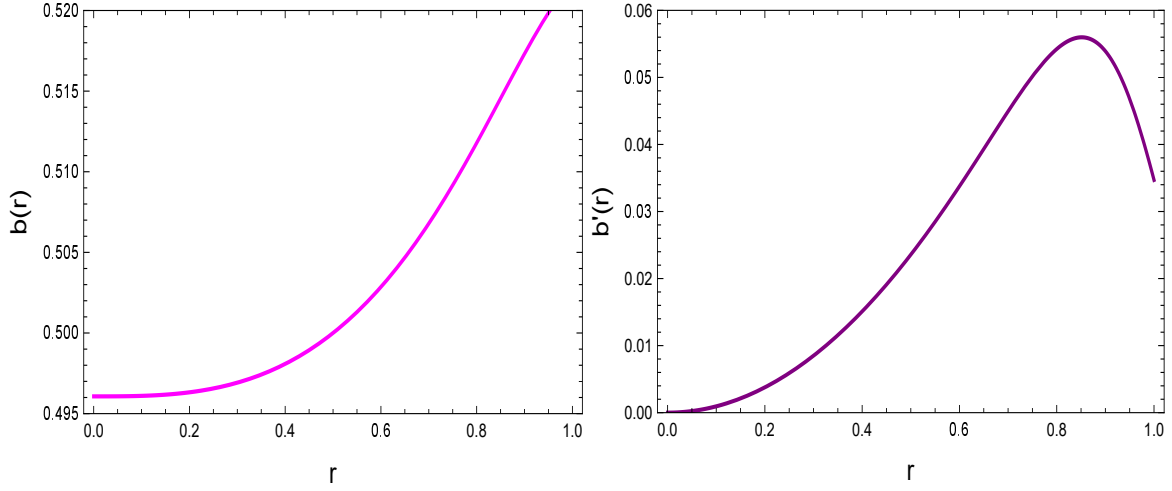


FIG. 13: The trajectory of $b(r)$ and $b'(r)$ versus r axis in $f(R)$ gravity.

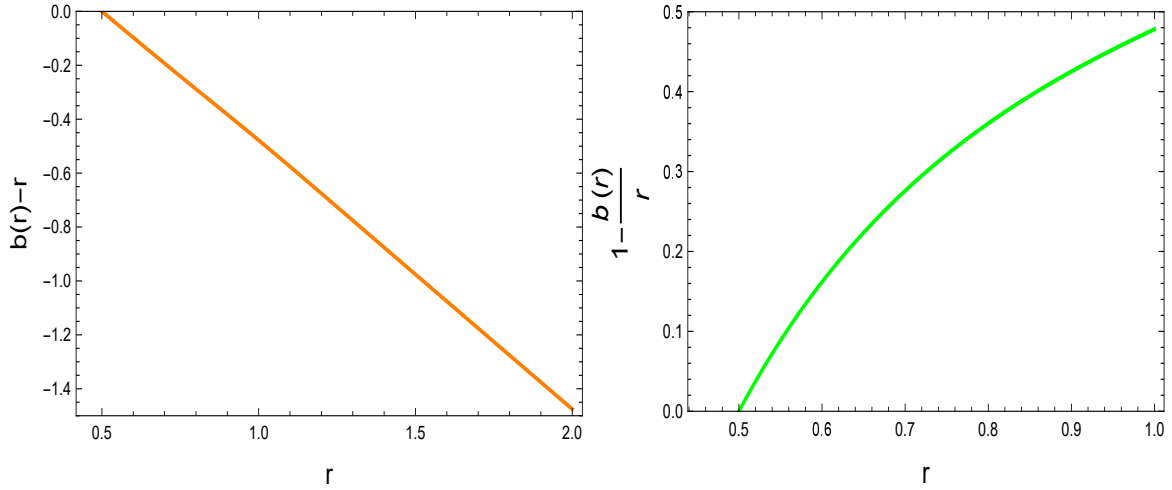


FIG. 14: The trajectory of $b(r) - r$ and $1 - \frac{b(r)}{r}$ along r in $f(R)$ gravity.

- [23] S. Nojiri and S. D. Odintsov, Phys. Rep. **505**, 59 (2011).
- [24] T. P. Sotiriou and V. Faraoni, Rev. Mod. Phys. **82**, 451 (2010).
- [25] S. Capozziello and M. De Laurentis, Phys. Rep. **509**, 167 (2011).
- [26] S. Capozziello and V. Faraoni, *Beyond Einstein gravity: A Survey of gravitational theories for cosmology and astrophysics*, vol. 170 (Springer Science & Business Media, 2010).
- [27] A. Joyce, B. Jain, J. Khoury, and M. Trodden, Phys. Rep. **568**, 1 (2015).
- [28] K. Koyama, Rep. Prog. Phys. **79**, 046902 (2016).
- [29] S. Nojiri, S. D. Odintsov, and V. K. Oikonomou, Phys. Rep. **692**, 1 (2017).
- [30] Z. Yousaf, K. Bamba, M. Z. Bhatti, and U. Farwa, arXiv preprint [arXiv:2311.10369](https://arxiv.org/abs/2311.10369) (2023).
- [31] L. Sebastiani and S. Zerbini, Eur. Phys. J. C **71**, 1 (2011).
- [32] T. Multamäki and I. Vilja, Phys. Rev. D **74**, 064022 (2006).
- [33] S. H. Hendi, Int. J. Theor. Phys. **53**, 4170 (2014).
- [34] T. Multamäki and I. Vilja, Phys. Rev. D **76**, 064021 (2007).
- [35] G. Nashed and E. N. Saridakis, Phys. Rev. D **102**, 124072 (2020).
- [36] G. G. L. Nashed and S. Nojiri, Phys. Lett. B **820**, 136475 (2021).
- [37] G. G. L. Nashed and S. Capozziello, Phys. Rev. D **99**, 104018 (2019).
- [38] A. de La Cruz-Dombriz, A. Dobado, and A. Maroto, Phys. Rev. D **80**, 124011 (2009).
- [39] S. C. Jaryal and A. Chatterjee, Eur. Phys. J. C **81**, 1 (2021).
- [40] E. F. Eiroa and G. Figueroa-Aguirre, Phys. Rev. D **103**, 044011 (2021).

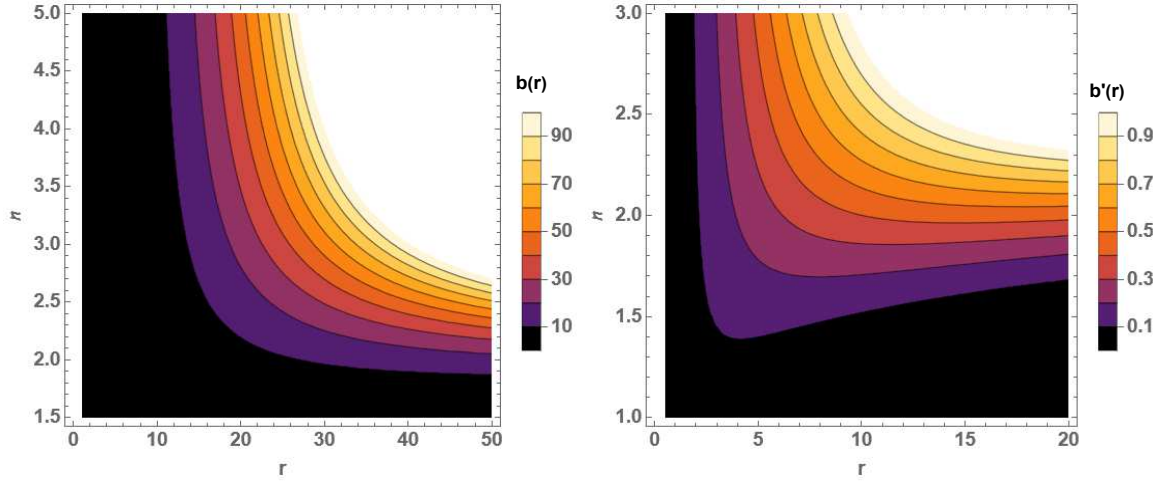


FIG. 15: The contour plots of $b(r)$ and $b'(r)$ for certain domain of n in $f(R)$ gravity.

- [41] Z.-Y. Tang, B. Wang, and E. Papantonopoulos, *Eur. Phys. J. C* **81**, 1 (2021).
- [42] Z. Yousaf, A. Adeel, S. Khan, and M. Z. Bhatti, *Chin. J. Phys.* **88**, 406 (2023).
- [43] Z.-Y. Tang, B. Wang, T. Karakasis, and E. Papantonopoulos, *Phys. Rev. D* **104**, 064017 (2021).
- [44] T. Karakasis, E. Papantonopoulos, Z.-Y. Tang, and B. Wang, *Phys. Rev. D* **103**, 064063 (2021).
- [45] T. Karakasis, E. Papantonopoulos, Z.-Y. Tang, and B. Wang, *Eur. Phys. J. C* **81**, 1 (2021).
- [46] S. Pi, Y.-l. Zhang, Q.-G. Huang, and M. Sasaki, *J. Cosmol. Astropart. Phys.* **2018**, 042 (2018).
- [47] A. De La Cruz-Dombriz, E. Elizalde, S. D. Odintsov, and D. Saez-Gomez, *J. Cosmol. Astropart. Phys.* **2016**, 060 (2016).
- [48] F. S. Lobo and M. A. Oliveira, *Phys. Rev. D* **80**, 104012 (2009).
- [49] C. Bejarano, E. F. Eiroa, and G. Figueroa-Aguirre, *Eur. Phys. J. C* **81**, 1 (2021).
- [50] E. F. Eiroa and G. F. Aguirre, *Eur. Phys. J. C* **76**, 1 (2016).
- [51] M. F. Shamir and I. Fayyaz, *Eur. Phys. J. C* **80**, 1 (2020).
- [52] S. V. Chervon, J. C. Fabris, and I. V. Fomin, *Class. Quant. Grav.* **38**, 115005 (2021).
- [53] T. Tangphati, A. Chatrabhuti, D. Samart, and P. Channuie, *Phys. Rev. D* **102**, 084026 (2020).
- [54] G. Mustafa, Z. Hassan, P. H. R. S. Moraes, and P. K. Sahoo, *Phys. Lett. B* **821**, 136612 (2021).
- [55] M. R. Mehdizadeh, M. K. Zangeneh, and F. S. Lobo, *Phys. Rev. D* **91**, 084004 (2015).
- [56] P. Kanti, B. Kleihaus, and J. Kunz, *Phys. Rev. D* **85**, 044007 (2012).
- [57] H. Maeda and M. Nozawa, *Phys. Rev. D* **78**, 024005 (2008).
- [58] S. Nojiri and S. D. Odintsov, *Phys. Lett. B* **631**, 1 (2005).
- [59] S. Nojiri, S. D. Odintsov, and V. K. Oikonomou, *Phys. Rev. D* **109**, 044046 (2024).
- [60] E. Elizalde, S. Nojiri, S. D. Odintsov, and V. K. Oikonomou, *arXiv preprint arXiv:2312.02889* (2023).
- [61] W. Luo, C. Liu, and Z.-K. Guo, *Eur. Phys. J. C* **84**, 394 (2024).
- [62] S. Nojiri, S. D. Odintsov, and V. K. Oikonomou, *Phys. Rev. D* **99**, 044050 (2019).
- [63] M. Dehghani and Z. Dayyani, *Phys. Rev. D* **79**, 064010 (2009).
- [64] M. K. Zangeneh, F. S. Lobo, and M. H. Dehghani, *Phys. Rev. D* **92**, 124049 (2015).
- [65] C. Lanczos, *Ann. Math.* p. 842 (1938).
- [66] D. Lovelock, *J. Math. Phys.* **13**, 874 (1972).
- [67] S. Nojiri, S. D. Odintsov, V. K. Oikonomou, and A. A. Popov, *Nucl. Phys. B* **973**, 115617 (2021).
- [68] D. Glavan and C. Lin, *Phys. Rev. Lett.* **124**, 081301 (2020).
- [69] R. Kumar and S. G. Ghosh, *J. Cosmol. Astropart. Phys.* **07**, 053 (2020).
- [70] Z. Haghani, *Phys. Dark Universe* **30**, 100720 (2020).
- [71] P. G. S. Fernandes, P. Carrilho, T. Clifton, and D. J. Mulryne, *Class. Quantum Grav.* **39**, 063001 (2022).
- [72] C. M. A. Zanoletti, B. R. Hull, C. D. Leonard, and R. B. Mann, *J. Cosmol. Astropart. Phys.* **01**, 043 (2024).
- [73] G. G. L. Nashed and S. Nojiri, *Eur. Phys. J. C* **83**, 68 (2023).
- [74] D. Lovelock, *J. Math. Phys.* **12**, 498 (1971).
- [75] B. Zwiebach, *Phys. Lett. B* **156**, 315 (1985).
- [76] J. Einasto, *Astron. Nachr.* **291**, 97 (1969).
- [77] J. Einasto, *Astrofizika* **5**, 137 (1969).
- [78] J. Einasto, in *Proceedings of the First European Astronomical Meeting Athens, September 4–9, 1972: Volume 2: Stars and the Milky*

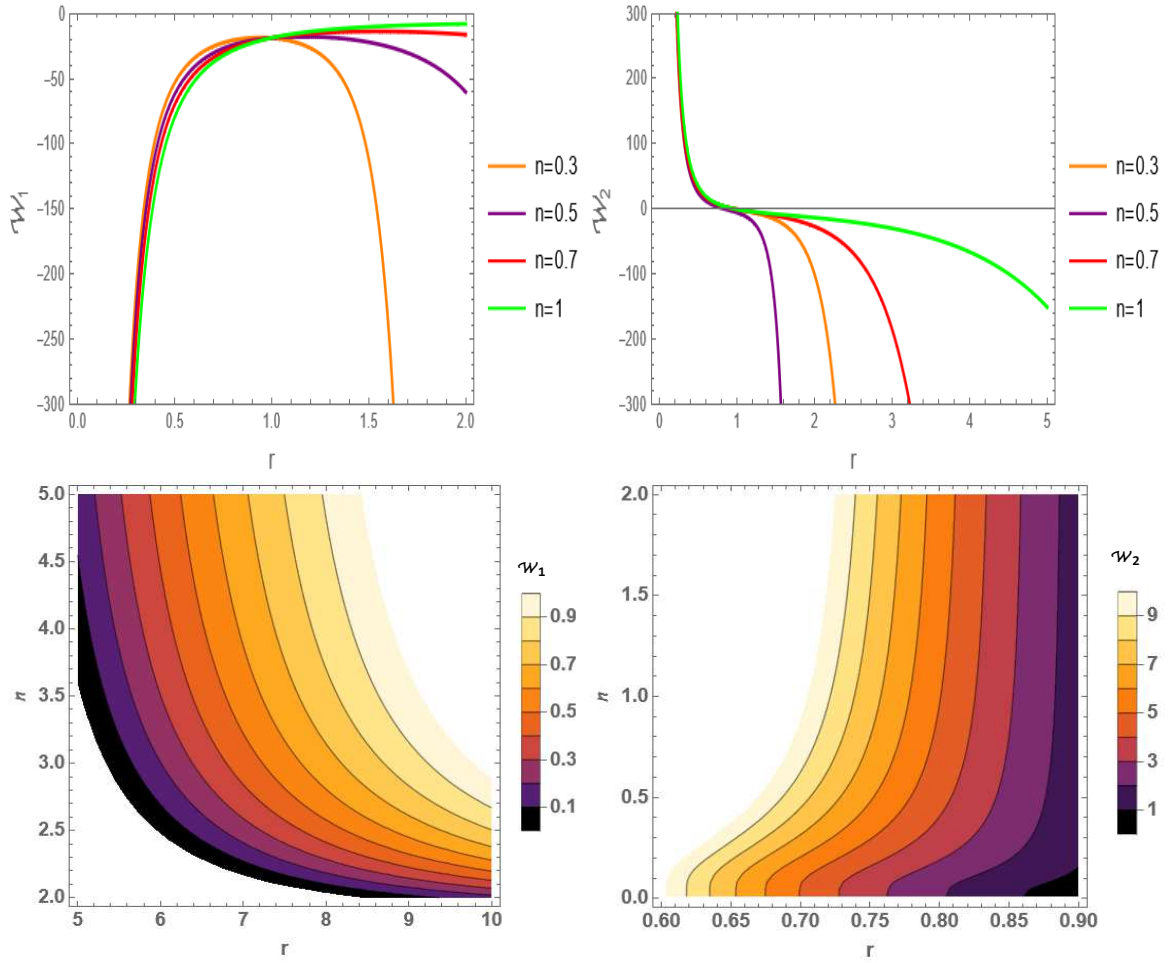


FIG. 16: w_r and w_t along radial axis r for some values of Einasto index n in $f(R)$ gravity.

Way System (Springer, 1972), p. 291.

- [79] L. Herrera, A. Di Prisco, E. Fuenmayor, and O. Troconis, *Int. J. Mod. Phys. D* **18**, 129 (2009).
- [80] L. Herrera, W. Barreto, A. Di Prisco, and N. Santos, *Phys. Rev. D* **65**, 104004 (2002).
- [81] S. D. Odintsov and V. K. Oikonomou, *Phys. Dark Universe* **32**, 100805 (2021).
- [82] V. K. Oikonomou, *Class. Quantum Grav.* **41**, 085008 (2024).
- [83] D. Merritt, A. W. Graham, B. Moore, J. Diemand, and B. Terzić, *Astron. J.* **132**, 2685 (2006).
- [84] L. Herrera, A. Di Prisco, J. Martin, J. Ospino, N. Santos, and O. Troconis, *Phys. Rev. D* **69**, 084026 (2004).
- [85] Z. Yousaf, M. Z. Bhatti, S. Khan, and P. K. Sahoo, *Phys. Dark Universe* **36**, 101015 (2022).
- [86] H. A. Buchdahl, *Mon. Not. R. Astron. Soc.* **150**, 1 (1970).
- [87] A. A. Starobinsky, *Phys. Lett. B* **91**, 99 (1980).
- [88] A. De Felice and S. Tsujikawa, *Living Rev. Rel.* **13**, 1 (2010).
- [89] G. Cognola, E. Elizalde, S. Nojiri, S. Odintsov, L. Sebastiani, and S. Zerbini, *Phys. Rev. D* **77**, 046009 (2008).
- [90] B. Li and J. D. Barrow, *Phys. Rev. D* **75**, 084010 (2007).
- [91] S. Nojiri and S. D. Odintsov, *Phys. Lett. B* **657**, 238 (2007).
- [92] E. Hayashi and S. D. White, *Mon. Not. R. Astron. Soc.* **388**, 2 (2008).
- [93] L. Gao et al., *Mon. Not. R. Astron. Soc.* **387**, 536 (2008).
- [94] J. F. Navarro et al., *Mon. Not. Roy. Astron. Soc.* **402**, 21 (2010).
- [95] P. F. de Salas, K. Malhan, K. Freese, K. Hattori, and M. Valluri, *J. Cosmol. Astropart. Phys.* **2019**, 037 (2019).
- [96] D. A. Gadotti, *Mon. Not. Roy. Astron. Soc.* **393**, 1531 (2009).
- [97] J. F. Navarro, C. S. Frenk, and S. D. M. White, *Astrophys. J.* **490**, 493 (1997).
- [98] E. Retana-Montenegro, E. Van Hese, G. Gentile, M. Baes, and F. Frutos-Alfaro, *Astron. Astrophys.* **540**, A70 (2012).
- [99] M. Baes, *Astron. Astrophys.* **667**, A47 (2022).

- [100] G. Cognola, E. Elizalde, S. Nojiri, S. D. Odintsov, and S. Zerbini, *J. Cosmol. Astropart. Phys.* **2005**, 10 (2005).
- [101] M. Sharif and Z. Yousaf, *Phys. Rev. D* **88**, 024020 (2013).
- [102] A. M. Albalahi, Z. Yousaf, A. Ali, and S. Khan, *Eur. Phys. J. C* **84**, 9 (2024).
- [103] Z. Yousaf, *Phys. Scr.* **95**, 075307 (2020).
- [104] S. K. Maurya, M. Govender, G. Mustafa, and R. Nag, *Eur. Phys. J. C* **82**, 1006 (2022).
- [105] J. Andrade, *Eur. Phys. J. C* **82**, 266 (2022).
- [106] P. León and C. Las Heras, *Eur. Phys. J. C* **83**, 260 (2023).
- [107] J. Andrade and D. Santana, *Eur. Phys. J. C* **83**, 523 (2023).